Final Report

Forensic Analysis of Building Materials Obtained by Core Drilling; Fort Sumter National Monument

by

Denis A. Brosnan
Professor, Clemson University

Sponsored By

The Southeastern Cooperative Ecosystems Studies Unit
The National Park Service
TASK Agreement J5430090029-Mod. 2
Cooperative Agreement Number H5000085050

June 26, 2012

Executive Summary

Masonry materials were obtained from core drilling of wallks in Fort Sumter National monument where the main purpose was determining physical properties of the materials for use in structural modelling of the fort. The materials were also characterized as to their chemical and mineralogical composition to aid on furture preservation and restoration efforts. A particular emphasis of this research was determining any evidence of deterioration of the materials.

The materials included clay bricks, masonry mortar, and concrete all of 1850 vintage as used in the Fort construction. The bricks were found to be of two types with the majority of bricks being the Charleston Grey type that also constitute the outer Fort walls. Bricks called Charleston Browns were also found in this study. The masonry mortars were constituted of sand, lime, and natural cement (aka historic Rosendale cement). While the original Fort was designed with through the wall brick masonry construction, tabby concrete infill was used within the walls to speed construction, as motivated by foreign threats of the era.

The most important deterioration found in this study was alkali-silica reaction or "ASR" within the tabby concrete materials. The ASR led to cracking within the concrete implying that the strength and elasticity of the concrete today are much lower than in original construction. This finding has important consequences on the structural modelling effort of the overall project.It is possible that the finding of ASR at Fort Sumter represents the oldest structure with documented occurance of ASR in north America.

Further, the marine environment encouraged diagenesis of the masonry mortars. This process is the formation of new mineral phases within the mortars over time thus altering their mineralogical compositions. The process of diagenesis of mortars is considered as a minor threat to the Fort's structure.

The results of this project are useful in preservation and restoration in the following ways:

- The composition of repair and restoration materials is revealed for use in future construction activities where authenticity of materials is of importance.

- Bricks in repairs should have a similar thermal expansion characteristic as the original bricks to ensure that no harm is done to the structure. It is also well-known that repair bricks should exhibit a similar modulus of elasticity as the original bricks.

Notice

As a courtesy to the reader of this report who is a practitioner, each section ends with a summary in non-technical language. Therse sections are indicated by the presence of a "light bulb" symbol. Persons not interested in the details of the analyses may choose to first read these special sections.

Introduction

Statement of Purpose

This research is a supporting component of the project entitled *Evaluate Fort Sumter Bricks and Mortars* sponsored by the National Park Service[1]. The overall project is described in an introduction in a technical paper authored by Dr. Sez Atamturktur[2] as:

"This manuscript presents a multi-faceted approach toward developing numerical structural analysis models of Fort Sumter in Charleston, South Carolina. The input parameters for the model are obtained from a series of field investigations including three-dimensional laser scanning, material testing of cored samples, and vibration tests. The model is calibrated to accurately represent the measured dynamic characteristics of the fort and is substantiated with loading scenarios, which represent historical events that affected the structure. With the established model, potential load scenarios due to wind, foundation settlement and earthquake are simulated to assess the structural integrity of the fort."

The purpose of this supporting component of the research is to characterize materials from core drilling specimens using advanced methods of chemical, mineralogical, physical, and petrographic analysis. The key questions addressed in this research are as follows:

1. *What are the compositions and structures of the materials, and how do they relate to previous studies of masonry materials found at Fort Sumter National Monument[3]?*

2. *What evidence is there of deterioration of materials by chemical or physical agents such that the physical properties of the materials, i.e. strength and elasticity, might be affected?*

---

[1] Support via the Piedmont-South Atlantic Cooperative Ecosystems Studies Unit, Statement of Work Between the National Park Service and Clemson University, Partner, H5000 08 5050, Task Agreement Number J5430090029-Mod. 2, Cooperative Agreement Number H5000085050.

[2] "Structural Assessment of Fort Sumter National Monument: On-Site Inspection, Model Development and Predictive Assessment," Sez Atamturktur, Saurabh Prabhu, Denis Brosnan, and Rick Dorrance, Submitted for publication in *Construction and Building Materials*, May 2012.

[3] Denis A. Brosnan, *Characterization and Forensic Studies of Construction Materials from Fort Sumter National Monument*, Report Prepared Under the Piedmont – South Atlantic Coast Cooperative Ecosystems Studies Unit Task Agreement for the National Park Service (2010).

Experimental Methods

Materials were characterized using techniques such as X-ray fluorescence spectroscopy or "XRF" (for chemical analysis), X-ray diffraction or "XRD" (for mineralogy), differential scanning calorimetry (DSC) and thermogravimetric analysis (TGA) with evolved gas analysis by Fourier transform spectroscopy (FTIR), mercury intrusion porosimetry (MIP), and determination of water soluble salts by ion chromatrography (IC), and these techniques are well described in the literature[4].

Analysis of cementitious materials was accomplished using procedures in ASTM C 1324-10, *Standard Test Method for Examination and Analysis of Hardened Masonry Mortar*. The analysis of mortars and concrete included petrographic or microscopic methods that are well-known research tools[5]. The petrographic analysis was supplemented using scanning electron microscopy (SEM)[6]. The instrumental methods are similar to those used by Chairi, et. al,[7] and the petrography follows techniques used by Walsh[8].

The analysis techniques of this study are commonly used in analysis of cement, ceramics, mortar, and concrete. With respect to the mortar and microscopy, standard methods of analysis were employed. It is not necessary to understand the analytical techniques in order to gain useful knowledge for preservation and restoration.

---

[4] See *Characterization Techniques for Ceramists*, Dennis R. Dinger, ISBN 0-9715696-6-5, Morris Publishing (2005).

[5] *Petrography Applied to Concrete and Concrete Aggregates*, Erlin/Stark Editors, ASTM STP 1061, ISBN 0-8031-1452-4 (1990). See also ASTM C 856-11, *Standard Practice for Petrographic Examination of Hardened Concrete.*

[6] SEM analysis followed ASTM C 1723-10, *Standard Guide for Examination of Hardened Concrete Using Scanning Electron Microscopy.*

[7] Chiari, G., Torraca, G., and Santarelli, M. L., "Recommendations for Systematic Instrumental Analysis of Ancient Mortars: The Italian Experience," Standards for Preservation and Rehabilitation, ASTM STP 1258, S. J. Kelley, Ed., American Society for Testing and Materials, (1996), pp. 275-284.

[8] John J. Walsh, *Petrography: Distinguishing Natural Cement from Other Binders in Historical Masonry Construction Using Forensic Microscopy Techniques*, Journal of ASTM International, Vol. 4, No. 1, pp. 20-31 (2007).

Specimen Information

Specimens were obtained from sequential core drilling operations of the Fort per Figure 1, with drilling accomplished in the latter part of 2011. Information on the cores is provided in Table 1. Cores were 2" (50 mm) in diameter, and drilling was by wet (water lubrication) or dry (air swept) methods. The term wet/dry indicates initial use of dry drilling with later use of water lubrication when excessive heat build-up was noted.

The spcimen nomenclature is composed of a three letter combination such as X-Y-Z, where X represents the core number (location), Y inidcates the drill segment number (as one segment is approximately one core drill length), and Z indicates a portion of an individual segment (numbered starting with 1). Specimens for forensic examination were chosen based on a desire to examine all of the types of materials, i.e. mortar, concrete, and clay bricks, with more than one specimen included per material type.

Table 1: Summary of Core Observations

Core	Drilling Date	Wet or Dry	Observations
1			No materials analyzed.
2	10/26/11	Dry	Layers: 1 (inside exposed wall toward outside) brick, 2 mortar, 3 brick, 4 brick; 48" drill depth; Wall approximately 60" thick.
3	10/27/11	Wet	All brick, 49.5" drill depth.
4	10/27/11	Dry/Wet	Layers: 1 brick 17.5", 2 tabby concrete 42.5".
5	12/1/11	Wet	Appeared to be all brick in 51" drill depth. Subsequent investigation found brick and tabby concrete.
6	10/28/11	Dry/wet.	Layers: 1 brick and mortar 34.5", tabby concrete 17", brick and mortar 11".
7	10/26/11	Dry/wet	Layers: 1 brick approximately 16", 2 tabby concrete 24"

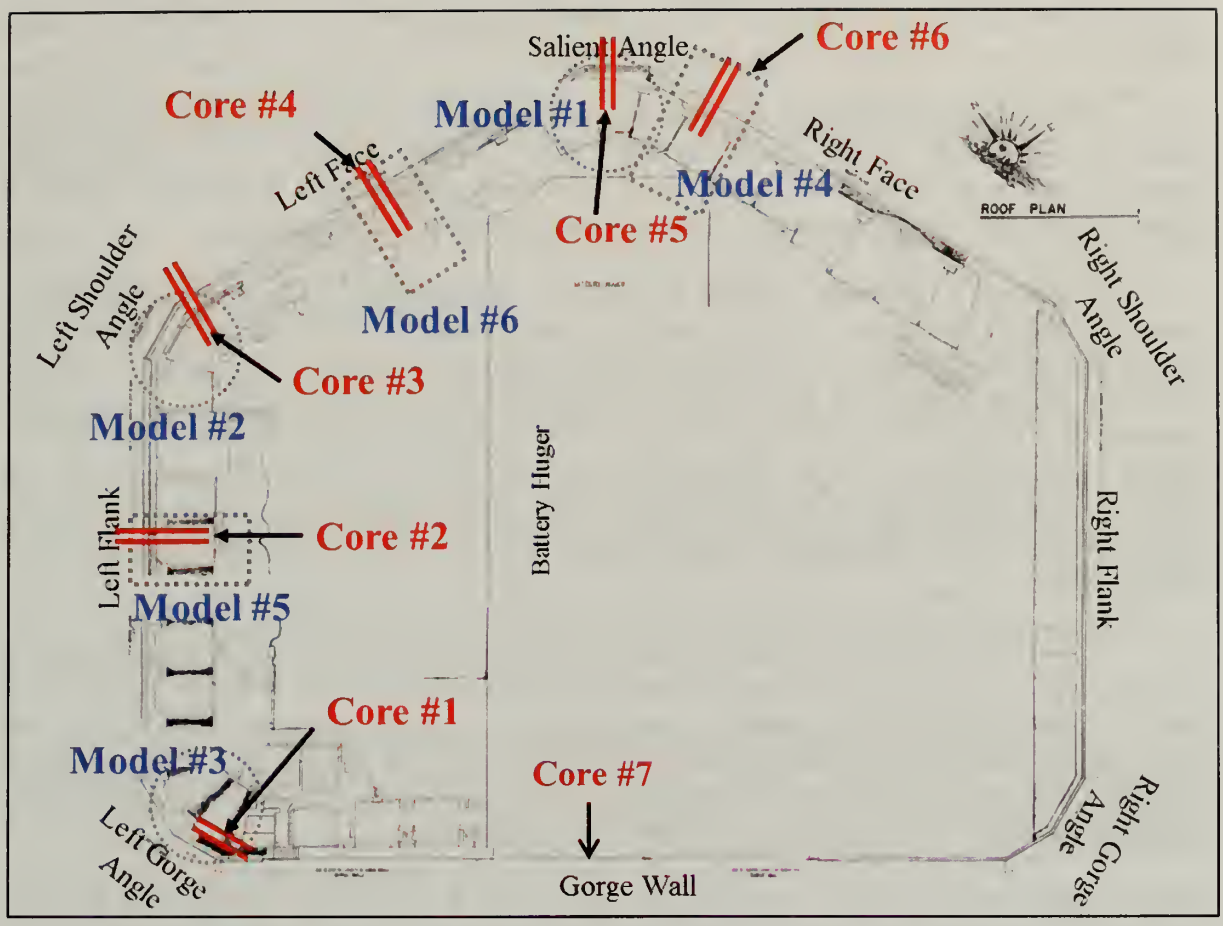

Figure 1: Core Drilling Locations

Characterization Results for Mortars and Concretes

Chemical and Mineralogical Characterization

The chemical, mineralogical, and physical data for the cementitious materials is given in Table 2. The "bulk XRF" provides the overall composition of the specimen (binder and agggregate), while the insoluble residue or "IR" provides the composition of the solid residual after acid treatment in the method of ASTM C 1324. Since C 1324 employs muriatic acid (hydrochloric acid), the residue is considered as the "sand" component of masonry mortar, i.e. as appropriate for mortars not containing acid soluble aggregates such as oyster shells. For tabby concretes, the insoluble residue includes sand plus any residuals from solution of the oyster shells.

The chemical analyses for the mortars 2-1-3 and 3-1-14 exhibit 74-76% silica (SiO_2) and 14-17% lime (CaO) with magnesia (MgO) and alumina (Al_2O_3) as minor composnents. By contrast, the tabby concretes 4-2-22 and 7-2-3 exhibit silica contents of 55.20% and 30.39% respectively reflecting lower sand contents in the concrete composition as compared to the

mortar compositions. Specimen 6-1-25 was found to more similar to mortar than to tabby concrete.

Photographs of specimens obtained by core drilling are shown in Figures 2-7. Tabby concretes are clearly distinguishable by their shell content (Figures 5-7); however, shell fragments can be found in the masonry mortar specimens originating in incomplete burning of shells in producing oyster lime and/or in job site contamination (See Figure 3).

In addition to chemical analysis, mortars were characterized as to their mineralogy by quantitative XRD (Figures 8, 12, 17, 24, and 29). The mineralogy of all materials included quartz (sand), calcite (from carbonation of lime after initial construction of the fort) and from shells as might be present, and trace quantities of amorphous (non-crystalline materials) and other (unidentified phases). Only tabbly concrete 7-2-1 contained identifiable trace minerals as kieserite [$MgSO_4(H_20)$], leucite ($KAlSi_2O_6$), and microcline ($KAlSi_3O_8$). Both leucite and mccrocline are likely related to the presence of clay brick fragments or "brick dust" in the mortar, while kieserite may reflect intrusion of sea water into the masonry materials in Core 7 (gorge wall).

Differential scanning calorimetry traces with evolved gas observations are presented in Figures 9, 13, 18, 25, and 30. All specimens exhibited decomposition of ettringite (123-162°C), brucite (349-381°C), the polymorphic transformation of α- to β-qaurtz (576-577°C), and decomposition of calcite (in two regimes of 655-694 °C and 758-863°C). The phase iowaite is suggested in mortar 2-1-3 by a water evolution at 550 °C (as well as a suggestion of iowate in the other specimens). All of these phases are described as follows:

Calcite – the mineral calcium carbonate or $CaCO_3$ that is a primary constituent of masonry mortars and concretes constituted of lime, sand, and sea shells. In cementitious materials, calcite is formed by reaction between quicklime [$Ca(OH)_2$] and carbon dioxide (CO_2) in the air providing for a set condition in the mortar. This calcium carbonate is cryptocrystalline (composed of small crystals) allowing it to decompose at lower temperatures on heating as compared to coarsely crystalline calcium carbonate as found in limestone, the latter of which decomposes at temperatures approaching 880°C. In the present study, all cementitious materials exhibited a low temperature carbonate peak (as from carbonation of lime in-situ after construction) and a high temperature peak (as from decomposition of oyster shells within the mortar). The influence of crystallinity on calcite decomposition has been reported by Beruto[9]. Further, the form of calcium carbonate in shells is aragonite, a phase that is transformed during thermal analysis to calcite on heating to in the range 450-520°C. This fact, considered along with the coarsely crystalline nature of marine shells, adds credence to the observation of high temperature calcite decomposition as observed in this study.

[9] Y.-L. Ren, *The Influence of Morphology of Ultrafine Calcite Particles on Calcite Decomposition Kinetics*, Journal of Thermal Analysis and Calorimetry 91 (2008) 867-871.

Ettringite – a mineral of the composition $3CaO\text{-}Al_2O_3\text{-}3CaSO4\text{-}31H_2O$ formed in the initial setting of cementitious materials[10] and potentially formed in-situ during the service of portland cement concretes, the latter called "delayed ettringite". The formation of delayed ettringite in cementitious materials involves expansions that are known to cause cracking and failure in materials.

Brucite – the mineral magnesium hydroxide or $Mg(OH)_2$. Brucite forms in-situ from soluble magnesium originating in masonry materials and from magnesium in sea water. Brucite has a well-defined thermal analysis profile[11].

Quartz – the normal form of crystalline silica as "sand" in the earth's crust that undergoes a change in crystal structure on heating at about 573°C (known as a polymorphic inversion).

Iowaite – a complex hydrated and carbonated magnesium iron oxychloride mineral formed within the cementitous material over time. It was found in a periodically submerged mortar specimen from the outer walls of Fort Sumter National Monument in a previous study (Reference 3). The presence of iowaite usggests long term alteration of materials or "diagenesis" since it is not a native constituent of cements, limes, sand, or shells. The thermal analysis of iowaite is published[12].

Leucite and Microcline – these forms of potassium alumino-silicates reflect the presence of brick fragments within the mortars. It was common practice to add "underburned" brick particles to mortars prior to the era of portland cement (later 1800's)[13], and microcline has been previously reported in a Charleston structure[14]. The presence of the mineral leucite suggests that fragments from harder burned bricks are also present in the material.

---

[10] S. Anato, M. Duane, and I. Hassan., *DTA, TG, and XRD Studies of Sturmanite and Ettringite*, Canadian Mineralogist 35 (2005) 1403-1409.

[11] N. Kais, *$Mg(OH)_2$ Dehydroxylation – A Kinetic Stud by Controlled Rate Thermal Analysis*, Solid State Science 11 (2009) 1028-1034.

[12] R. L. Frost and K. L. Erickson, *Thermal Decomposition of Natural Iowaite*, Journal of Thermal Analysis and Calorimetry, 78 (2004) 367-373.

[13] The brick dust provided for pozzolanic properties in the mortar that include faster setting, thereby speeding construction, higher ultimate strength, and greater chemical resistance.

[14] Denis A. Brosnan, *Forensic Evaluation of Bricks and Mortar 17th Century Charleston Fortified Wall*, Work under the Piedmont – South Atlantic Coast Cooperative Ecosystem Studies Unit Task Agreement J5430090029, Modification 2, August 16, 2011 (Revised May 9, 2012).

The chemical and mineralogical studies revealed the following:

Mortar – the composition of mortar within the walls is similar to that used on the outer Fort walls, i.e. the compositions were cement, lime, and sand. The cement was identified as Rosendale natural cement by using the petrographic information dfiscussed later in this report.

Tabby Concrete – the tabby concrete was composed of oyster lime, sand, and shells. This material was used within the walls to save tiem and expense as an alternative to using the original design of through the wall brick masonry.

Deterioration – there was evidence of alteration of some materials over time through a process called diagenesis. This process is natural, and it does not represent a significant threat to the structure. Other forms of deterioration, as discussed later in this report, do represent significant concerns for the masonry materials.

Petrographic Analysis

The characterization of the mortar and concrete materials is further conducted using petrographic analysis to include classical thin section mineralogy and scanning electron microscopic examination. Various key microstructural features are described in the following:

a) Natural Cement in Mortars 2-1-3 and 3-1-14

Natural cement particles are found dispersed in the binder phase of mortar 3-1-14 (Left shoulder angle of FSNM) as shown in Figure 14. A relic (unreacted) cement particle is also seen in mortar 2-1-3 (left flank) as shown in Figures 10 and 11. These particles were from the Rosendale cement used in the composition. Since historic Rosendale cement was not a finely ground product[15], it is not unusual to see unreacted residuals in the mortar by petrographic microscopy (Reference 8).

b) Presence of Lime in the Binder Phase

[15] Natural cement was rarely ground to fineness less than 95% passing a 50-mesh sieve (opening 0.3 mm or 300 microns). See Cements, Limes, and Plasters, Edwin C. Eckel, Donhead Publishing (Reprint of 1928 Edition), ISBN 187339473X. p. 238.

A lime agglomerate is clearly visible in mortar 3-1-14 in Figures 15 and 16. The lime appears to be hollow [where residual $Ca(OH)_2$ dissolved leaving a periphery of calcite crystals]. In observation using crossed nicols (Figure 16), the carbonated phase appears as white crystals in the residual agglomerate. An intact lime agglomerate is seen in material 6-1-25 in Figure 19.

c) Presence of Shells in Tabby Concrete

A shell fragment is seen in tabby concrete 4-2-22 in Figure 26. The shell exhibits coloration in transmitted light due to birefringence, a consequence of crystalline anisotropicity[16]. In the same photomicrograph, the sand grain adjacent to the shell fragment exhibits peripheral corrosion suggesting alkali-silica reaction (ASR).

d) Salt Corrosion in 4-2-22

Evidence of salt related corrosion was found in tabby concrete 4-2-22, as shown by a darkened area to the lower left side of the photomicrograph in Figure 28. The mechanism is solution of calcite from the binder phase of the mortar by the action of intruding sea water. Similar evidence of corosion was found in the petrographic analysis of mortars from FSNM (Reference 3).

e) Brick Dust in 7-2-1

Brick dust was found in the binder phase of tabby concrete 7-2-1, as shown in Figures 31 and 32. The brick contributes soluble iron locally resulting in staining of the binder phase (Figure 32).

f) Specimen 6-1-25

This specimen had the macroscopic appearance of a mortar containing small shell fragments (Figure 4). The insoluble residue or sand contant of 58.6% also suggests a mortar composition (Table 2), but natural cement particles were not found in the microstructure (Figures 19-23). Larger shell fragments were not present in the microstructure. Therefore, the specimen was considered a lime-sand mortar composition.

[16] See http://en.wikipedia.org/wiki/Birefringence.

Petrographic (microscopic) studies provided the following key results:

Natural cement and lime in mortars – the cement was identified as histroic Rosendale natural cement, the same cement used on the Fort's outer walls.Lime relics were found in the mortar and concretes.

Evidence of salt corrosion was found in the mortar specimens from Core 4 from the Left Face (possibly original construction). Similar corrosion was found in earlier studies in mortars expossed to periodic sea water contact on the Fort walls.

Evidence was found of ASR in tabby concrete by petrography as cited above. ASR involves expansion reactions between alkali sources and siliceous aggregates that cause cracking within mortars and concrete[17]. ASR is usually diagnosed using petrographic techniques[18] with "global swelling" or three-dimensional expansion leading to crack initiation and propagation. The physical properties of the concrete – to include strength and elastic modulus – are likely affected by ASR. In this study, both tabby concrete specimens exhibited ASR, while one of three mortar specimens exhibited ASR.

The petrographic evidence for core 4-2-22, tabby concrete, is shown in Figure 26. The ASR has resulted in fragmentation at the immediate periphery of the quartz (sand), and a tell-tale crack is present in this microstructure. A similar phenomenon is seen in a mortar specimen in core 6-1-25 (Figure 20).

The results of examination of core 7-2-11 using scanning electron microscopy are given in Figure 33. The quartz sand chemistry is reflected in the energy dispersive X-ray analysis for Spectrum 4, where the sand exhibits about 98% SiO_2 and 1.7% CaO[19] By contrast, the fractured periphery of the sand grain (Spectrums 1 and 2) as a result of ASR exhibits a lesser quantity of silicon (or SiO_2), greater alkali (Spectrum 1), and substantially more calcium. The area bounded by Spectrum 3 is probably a shell fragment, while Spectrum 5 is the binder phase of calcium carbonate and/or natural cement in the concrete. Cracks are also seen in Figure 34 seemingly emanating from the periphery of the quartz grain – the consequence of global swelling at the periphery of the quartz.

Chlorine is detected in Spectrums 2 and 4 suggesting sea water infiltration of this material. It should be noted that detection of low levels of elements can be limited by the detection limits of the SEM/EDAX[20]. *This simply says a lack of detection does not necessarily mean an element is not present – it is simply below the detection limit.* Further, the EDAX is affected by the inherent inhomogeneous nature of early hand mixed mortars or concretes.

---

[17] P. Rivard, B. Fournier, and G. Ballivy, The Damage Rating Index Method for ASR Affected Concrete – A Critical Review of Petrographic Features of Deterioration and Evaluation Criteria, *Cement, Concrete, and Aggregates,* Vol. 24, No. 2, Paper ID CCA11228_242, Available online at: www.astm.org.

[18] P. Rivard, B. Fournier, and G. Ballivy, Quantitative Petrographic Technique for Concrete Damage due to ASR: Experimental and Application, *Cement, Concrete, and Aggregates,* CCAGDP, Vol. 22, No. 1, June 2000, pp. 63–72.

[19] A carbon level in the low pressure SEM of below 10% is usually attributed to carbon dioxide gas in the chamber interacting with the electron beam thereby generating carbon X-rays.

[20] EDAX is shorthand for Energy Dispersive X-ray Analysis, a technique common in electron microscopy.

The most interesting observation is that ASR was only found in those specimens not containing Rosendale cement, as follows:

Core Specimen with ASR	Material	Core Location
6-1-25	Masonry mortar with lime binder	Right Face
4-2-22	Tabby concrete with lime binder	Left Face
7-2-11	Tabby concrete with lime binder	Gorge Wall

This finding of ASR at FSNM may be for the earliest masonry construction in North America. Prior to this research, the "oldest" occurrence of ASR was apparently in an Endicott-era fort of 1890's vintage in New Hampshire[21].

These results strongly imply that the historic Rosendale cement in mortars 2-1-3 and 3-1-14 prevents or mitigates in the phenomenon of ASR. This is an extremely important observation with broad implications for historic preservation. It has been previously demonstrated that additions of metakaolin to Portland cement concretes affects the degree of ASR development and prevents ASR if the content of metakaolin in the concrete is present in substantial concentration[22]. Therefore, Rocendale cement may be functioning in a same manner as metakaolin to "protect" mortars subjected to a amrine environment.

Alkali-silica reaction (ASR) evidence was found in cementitious materials (concretes) within the Fort's walls. These expansive reactions cause cracking within the concrete that lowers the strength of the concrete and lowers its Modulus of Elasticity. This result is very significant, and structural modelling must take into consideration the consequences of ASR. In simple terms, the consequence of lowering the Modulus of Elasticity is that the inner walls are not as rigid as originally designed so that stresses within the walls result in larger deformations than expected. It is reasonable to consider that bonding between structural elements within the walls is affected leading to incomplete load transfer between elements and possible separation between layers.

It is possible that the finding of ASR at FSNM represents the oldest documentation of ASR in North America.

[21] Personal communication, Mr. Ray Rollins (Rollins Consulting), April 14, 2012.
[22] K. Gruber, T. Ramlochan, A. Boddy, R. Hooten, and M. Thomas, Increasing Concrete Durability with High-Reactivity Metakaolin, Cement and Concrete Composites, 23 (2001) 479-484.

Mortar Batch Compositions

The batch compositions for the mortars was determined using the protocol in ASTM C 1324 as a guide. The composition of tabby concretes was estimated using the quantitative mineralogical (XRD) and petrographic data. The results are given below in volumetric proportions:

	Mortar 2-1-3	**Mortar 3-1-14**	**Mortar 6-1-25**	**Tabby Concrete 4-2-22**	**Tabby Concrete 7-2-1**
Parts natural cement	1	1	½	0	0
Parts lime [$Ca(OH)_2$]	1.5	1	1	1	1
Parts sand	3	2	2	1	½
Parts shell	0	0	0	¾	½

The masonry mortars exhibit a binder to sand ratio of about one to one, and this was a typical volumetric proportion used by the U.S. Corps of Engineers with natural cement during the construction of Third System Fortifications. The mortar also contained lime, so the interior mortared elements employed a similar composition as those of the outer walls.

The tabby concrete compositions exhibited similar proportions of lime and sand with somewhat less proportion of shell fragments.

Characterization Results for Bricks

Chemical and Mineralogical Characterization

The core specimens of bricks are shown in Figures 35-40, with most bricks exhibiting black chert nodules that are typically found in "Charleston Grey" bricks refelcting their production on the sea islands around Charleston. The bulk of bricks on the walls of FSNM exhibit a similar appearance (Reference 3). The bricks shown in Figure 39 were possibly a type known as "Charleston Brown", a type possibly produced in the upper reaches of the Ashley or Cooper River estuaries and found in a minority of the bricks used on FSNM walls. The chemical, mineralogical, and physical data for the bricks is given in Table 5.

The primary chemical constituent in the bricks is silica (SiO_2), reflecting the extremely high content of sand in the coastal raw materials used in manufacture of the bricks. The silica is present in the crystalline forms quartz, tridymite, and cristobalite, wherein the high firing temperature of the bricks (required to achieve strength durability) exceeded about 1250°C leading to conversion of some quartz to tridymite and cristobalite[23]. By contrast, contemporary bricks made from clay or shale contain typically less than about 25% sand, and it is present as quartz due to firing temperatures below 1050°C.

The quartz content and other forms of crystalline silica in the bricks imparts a very high coefficient of linear expansion (CTE) to the bricks on the order of 9.5-12.5 exp (-6)/K. Such values of CTE are found in semi-silica refractory bricks, while contemporary clay bricks exhibit CTE values in the range 5-6 exp (-6)/K. It is vitally important that any bricks used to repair FSNM exhibit a similar CTE to ensure structural integrity.

The main coloring oxide in the bricks is iron (as Fe_2O_3). The bricks classified as "Greys"[24] are of a brown color shade, a typical result of the presence of CaO entrained in the brick making raw material. In the analyses in Table 5, the CaO levels are lower than ones found in the Grey bricks in the outer walls of FSNM (Reference 3) of about 0.5-0.6%. This suggests that second quality bricks could have been used for infill in the walls.

The amorphous phase detected in the bricks includes the crude glass formed in firing of the bricks and serves as the permanent "ceramic bond" in the bricks. This glass was formed at temepratures exceeding about 900°C, and on cooling of the bricks in the kiln it solidified. Another mineral called mullite ($3Al_2O_3{\cdot}2SiO_2$) is formed during firing of the bricks as the clay minerals decomposed. Mullite is a normal minor constituent of clay building bricks.

The bricks in Table 5 exhibit bulk densities of 1.54-1.67 g/cm^3, and bricks were of a similar denisty on the walls of FSNM. The apparent (open) porosities of the bricks used as infill (Table 5) and those on the outer walls were similar. The bricks used in infill were well-fired, as

---

[23] Brick makers in the Charleston, SC, area before 1860 used "Scotch kilns", i.e. rectangular downdraft kilns, to achieve the high temperatures needed to impart strength to the high quartz content sea island clays – unpublished work by Dr. Denis Brosnan, Clemson University.

[24] The bricks were called Greys due to their grey color when dried and before firing.

indicated by very low fractions of porosity less than one micron in size. The numbers on "fine pores" (<1 μ diameter) are so low (and lower generally than the brick on the outer walls) that they lend credence to the idea that "seconds" or second-quality bricks (as overfired bricks that might have been deformed in shape) were used in the infill.

The water soluble salts show that only one specimen (6-1-25) from the right face exhibits extremely high contents of species expected from sea water immersion. In fact, this specimen exhibits soluble sodium and chloride of a similar magnitued as a specimen from FSNM lower walls that saw periodic sea water contact by tidal flow (Reference 3 for Specimen 2 from the outer gorge wallks near the left gorge angle). It is possible that the infill of FSNM from late 1800's construction of Battery Huger using dredging spoils contributes to the salt level in Core 6 due the close proximety of the infill to this core. All other cores (Table 5) exhibit soluble salts as were found in upper FSNM walls.

Most of the bricks used within the Fort's walls were *Charleston Greys*, a type of brick manufactured on the sea islands around the Charleston Harbor. These same bricks were used to a large extent on the outer Fort walls. These were well-fired, as brick makers of the time used special kilns to achieve the high temepratures required by the sandy coastal clays.

Some *Charleston Brown* bricks were found within the walls. These bricks were less expensive during the era of the Fort construction. It is likely that the overseers "used any brick they could get" during construction.

No evidence of deterioration of bricks was found. Bricks from the right face contained high levels of water soluble salts. The proximity of infill near the coring position suggests that the infill is related to the salt content.

The most imoortant finding for restoration is that the bricks exhibit very high coefficients of linear thermal expansion. The density and pore structure of the bricks suggests that they exhibit high values of Modulus of Elasticity. Any bricks used in repair and restoration should have similar expansion and elasticity properties to ensure no future damage to the structure.

Petrographic Analysis

The petrographic analysis found two distinct microstructural types of bricks. One type was the Charleston Grey brick characterized by the presence of chert nodules or black granules visible on the surface of the brick or cut sections thereof. The other type of brick exhibited only a few or no black granules and a different microstructure suggesting strongly that it was the Charleston Brown brick.

Historical records show the sale of Grey, Brown, and Red types during the 1850's. The majority of brick buldings on the Charleston peninsula are built of grey bricks. Records indicate that the brown bricks were sold at a lower price than grey bricks suggesting that the brown bricks were considered as inferior. It is likely that the brown and red bricks were made from mineral concentrations of kaolin pottery clay located somewhat upriver from the penninsula and/or in the upcountry beyond the upper reaches of the Ashley or Cooper rivers[25]. This pottery clay did not contain chert nodules. Less is known of the red bricks, but similar colored bricks were produced in Dorchester County (SC) in the 1950's and 1960's.

a) Grey Bricks

Microstructural features of grey bricks are shown in Figures 41-48 and 54-56. In some cases, companion photomicrographs are taken using differing microscope techniques. As an example, a conventional reflected light photomicrograph is provided in Figure 42 while the same area using cross nicols is provided in Figure 42. With clay bricks, reflected light is a very convenient way to view the microstructure, and reflected light using crossed nicols shows the vitrified matrix as a colored area.

The bricks exhibit a substantioal amount of sand across their microstructure consistent with the finding of about 70-90% crystalline silica (sand) by quantitative XRD. It is obvious that there is a large amount of porosity present, and the pores are usually large in hand molded clay bricks. The vitreous matrix is of a limited extent in bricks with such a high quantity of sand in the composition.

The grey bricks are characterized by their content of chert nodules (See Figures 41-42, and 45-46). The chert originates with iron and sand rich nodules or concretions generally referred to a "plinthite" and found in hummus poor soils. On firing of the bricks, the plinthite nodules form chert-like agglomerates deriving their black color from the fayalite mineral ($2FeO{\cdot}SiO_2$) and iron spinel (Fe_3O_4) formed during firing by the reaction of iron oxide and quartz.

b) Brown Bricks

Microstructural features of brown bricks are shown in Figures 49-53. These bricks contain only a few chert nodules (as in Figure 49), and their vitrified phase contains iron spinel

[25] Brick making and whiteware pottery ("Carolina Creamware") were produced at Cainhoy and on Daniel Island. See Beyond God's Back, Herb Frasier, Evening Post Books, pp. 57-59 (2011).

crystals that appear as white angular features in reflected light (Figure 52). In reflected light with crossed nicols, the spinel crystals appear red and are concentrated near pore walls (Figure 53). This spatial orientation of spinel crystals suggests precipitation from the vitreous phase as the brick cooled, i.e iron oxide exsolved near pore walls forming crystals at the periphery. The high temperatures involved in brick firing resulted in defined reaction rims around some quart particles (Figure 50). These rims are not related to ASR seen in the mortars without natural cement in their composition.

The petrographic studies characterized the mineralogy of the bricks. They were high quartz content vitrified clay bricks made by hand molding, drying, and firing to temperatures of about 1250°C. They differ from contemporary bricks made of clay or shale, in that today's molded bricks usually contain less than about 25% sand with the consequence that contemporary bricks exhibit a lower coefficient of thermal expansion. For this reason, contemporary bricks of low thermal expansion coefficient should not be used in replacement or restoration of Fort Sumter National Monument.

Figure 2: FS Core Drill Mortar 2-1-3

Figure 3: Core Mortar 3-1-14

Figure 4: Core Mortar/Tabby Concrete 6-1-25

Figure 5: Core Tabby Concrete 4-2-22

Figure 6: Core Tabby Concrete 7-2-11

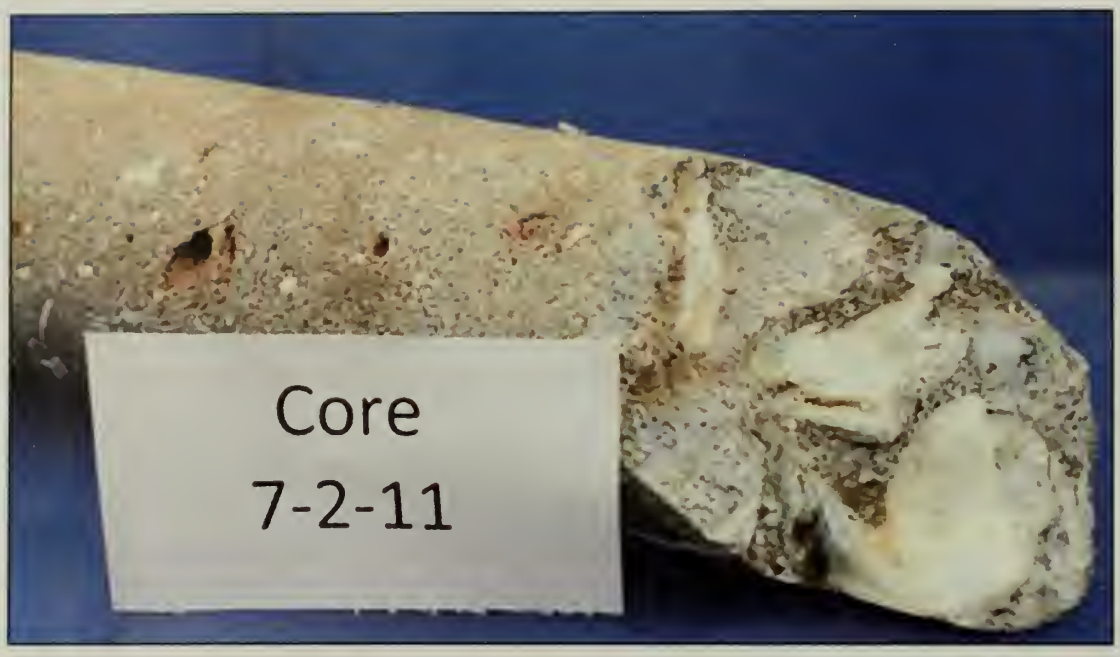

Figure 7 – Detail of Tabby Concrete Core 7-2-11

Table 2: Mortar and Concrete Analytical Data Summary

(M = mortar and TC = tabby concrete)

	2-1-3 M	3-1-14 M	6-1-25 M	4-2-22 TC	7-2-1 TC
Bulk XRF					
Al_2O_3	1.48	1.47	1.53	5.78	2.38
SiO_2	76.42	74.10	75.71	55.20	30.39
Na_2O	<0.5	<0.5	<0.5	<0.5	<0.5
K_2O	0.05	0.03	0.02	0.33	0.04
MgO	5.85	5.95	5.52	5.66	7.23
CaO	14.85	17.17	16.05	27.76	54.58
TiO_2	0.10	0.08	0.09	0.49	0.12
MnO	0.07	0.07	0.06	0.07	0.09
Fe_2O_3	0.81	0.82	0.77	2.38	0.98
P_2O_5	0.08	0.08	0.08	0.08	0.07
S	<0.05	<0.05	<0.05	1.93	3.56
Insoluble Residue XRF					
Al_2O_3	<0.1	<0.1	0.11	5.78	0.70
SiO_2	99.03	99.03	98.70	55.20	97.70
Na_2O	<0.5	<0.5	<0.5	<0.5	<0.5
K_2O	0.04	0.04	0.07	0.33	0.20
MgO	0.40	0.40	0.45	5.66	0.40
CaO	<0.01	<0.01	<0.01	27.76	0.20
TiO_2	0.08	0.06	0.08	0.49	0.10
MnO	0.01	0.01	0.01	0.07	0.02
Fe_2O_3	0.20	0.22	0.34	2.38	0.50
P_2O_5	0.08	0.09	0.09	0.08	0.08
Insoluble Residue, %	64.2	63.5	58.6	45.92	34.84
LOI	14.75	14.29	15.61	20.17	32.20
XRD, %					
Quartz	68.2	75.7	68.6	45.7	14.1
Calcite	28.4	21.3	27.4	36.6	77.1
Amorphous + Other	3.4	3.0	3.9	4.9	Note 1
Soluble Salts, ppm of dry specimen					
Na	2321	117	8154	2654	554
K	1643	229	1098	833	542
Mg					
Ca	1041	3932	3500	1675	9411
Cl	5991	1177	15689	4067	3774
NO_2	462	28	182	42	26
SO_4	323	2612	523	1225	1272
Bulk density, g/cm^3	1.63	1.90	1.63	1.68	1.80
Apparent Porosity, %	33.6	22.5	37.9	25.0	21.9
Fraction of pores <1 micron	69.5	87.0	81.0	80.7	88.4
Thermal Analysis					
Portlandite	N	N	N	N	-3.14
$MgCO_3$					-4.22
$CaCO_3$					-20.35

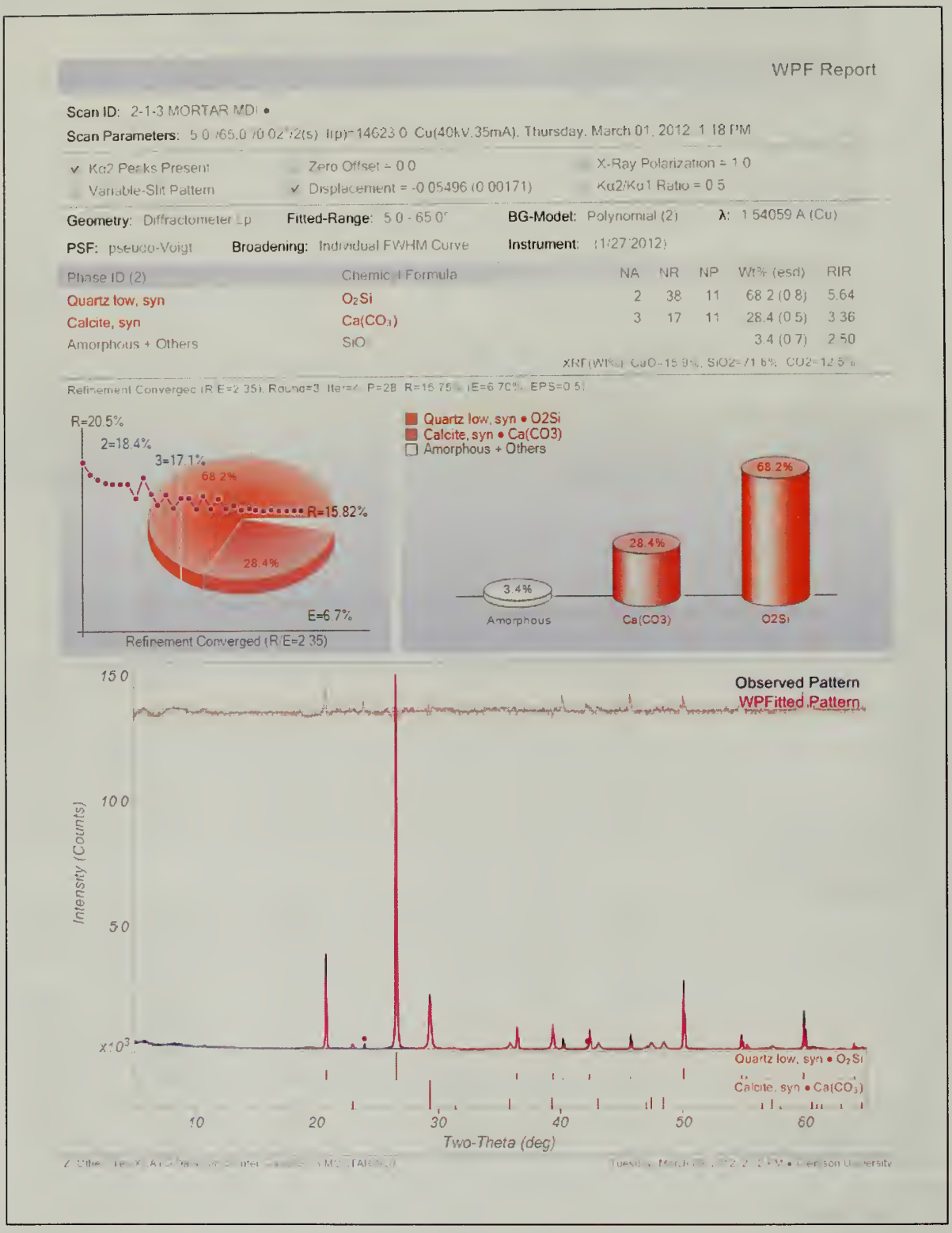

Figure 8: XRD of Mortar 2-1-3

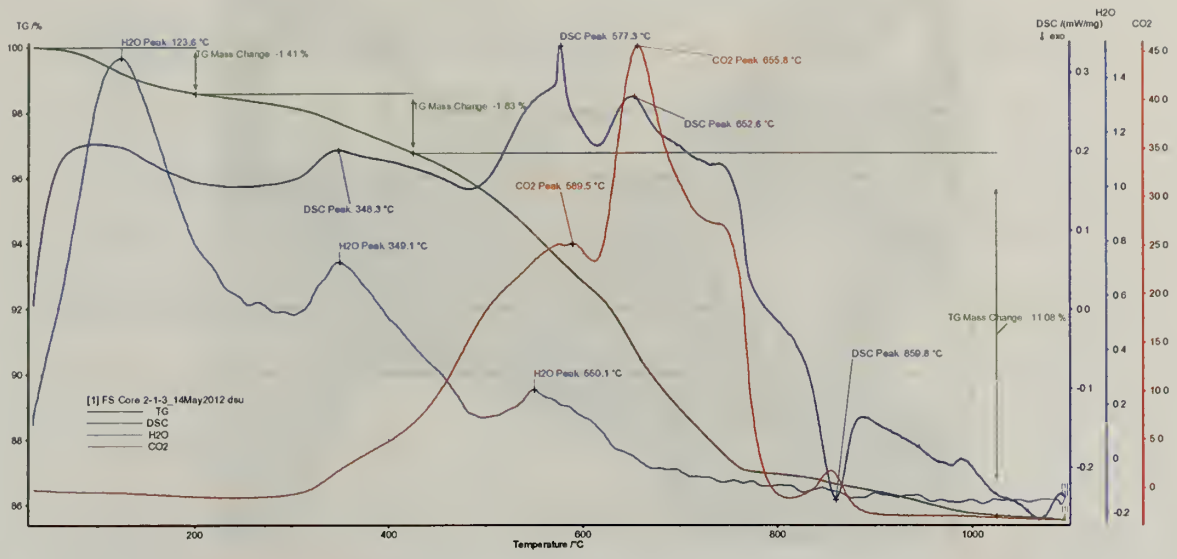

Figure 9: TGA/EGA of Mortar 2-1-3

Typical Thermal Events Observed in Thermal Analysis of Historic Bricks and Mortars (These events serve as a "fingerprint" for mineral identification)

Event Temperature (Approximate, °C)	Mineral Species Involved	Type of Event
120-149	Ettringite	Decomposition with water release
122, 200	Gypsum	Decomposition with water release
300-400	Brucite	Decomposition with water release
400-460	Portlandite	Decomposition with water release
551	Iowaite	Decomposition with water and CO2 release.
573	Quartz	α to β polymorphic transformation (crystal structure change)
620-690	Calcite	Typical decomposition for cryptocrystalline calcite formed due to in-situ carbonation of mortars.
680-800	Calcite	Typical decomposition for coarsely crystalline calcite in rock lime (as limestone) and marine shells.

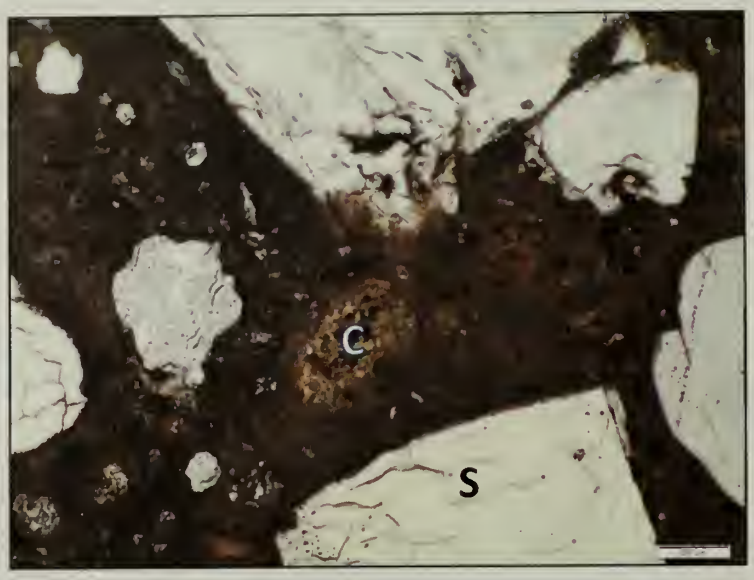

Figure 10: Microstructure of Mortar 2-1-3 with Cement Relic PPL

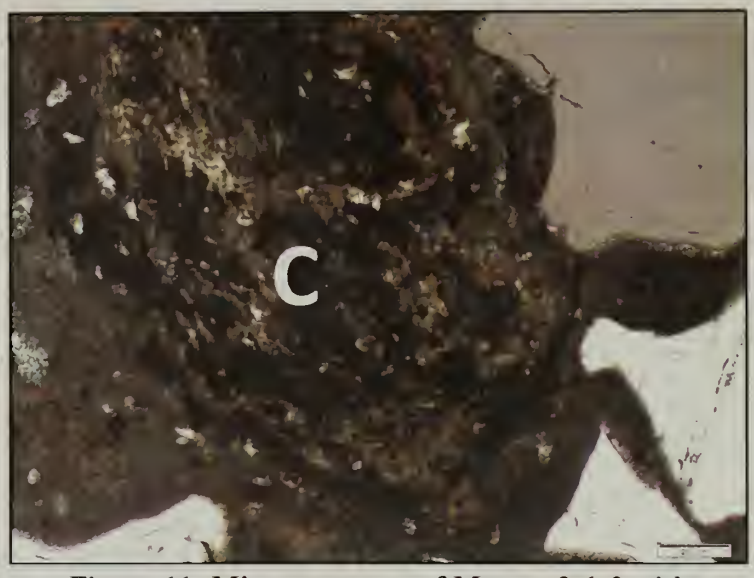

Figure 11: Microstructure of Mortar 2-1-3 with Detail of Cement Relic PPL

Microstructural Features: Sand (S), cementitious matrix (M), Pores (P), Lime relic (R) and Cement relic (C); PPL=plane polarized transmitted light and XPL=transmitted light crossed nicols.

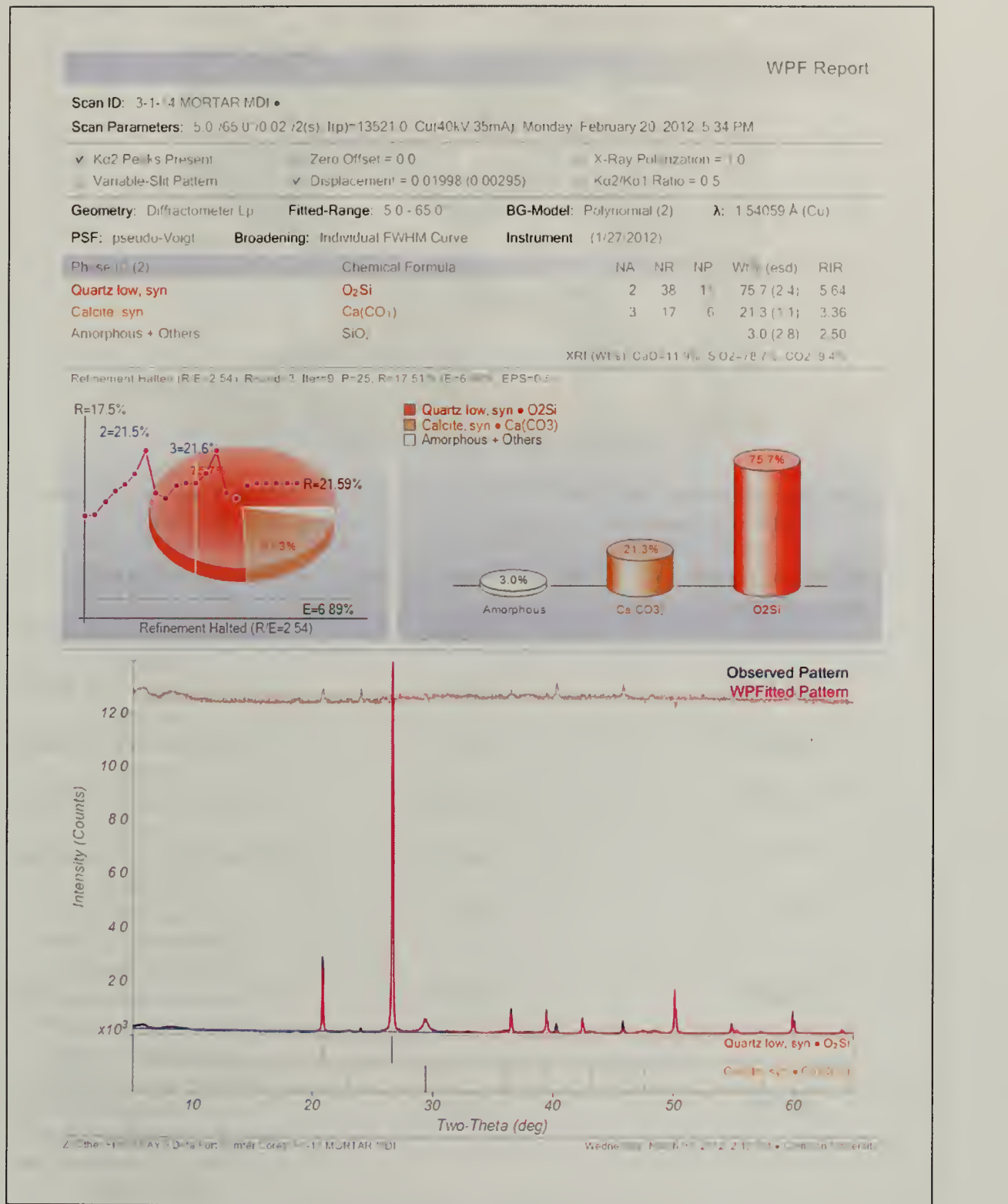

Figure 12: XRD of Mortar 3-1-14

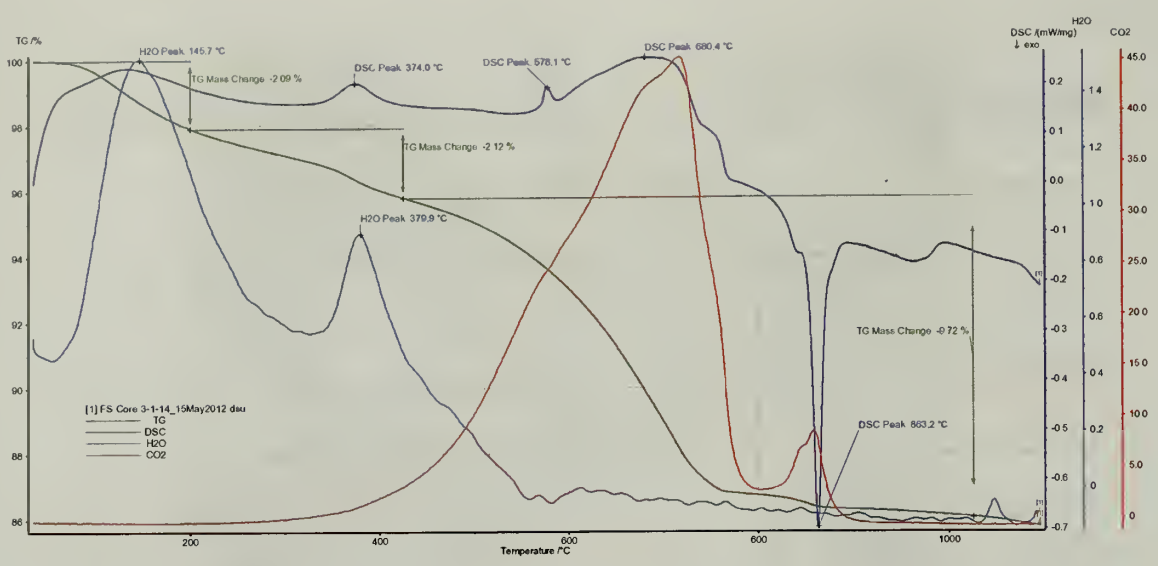

Figure 13: TGA/EGA of Mortar 3-1-14

Typical Thermal Events Observed in Thermal Analysis of Historic Bricks and Mortars (These events serve as a "fingerprint" for mineral identification)

Event Temperature (Approximate, °C)	Mineral Species Involved	Type of Event
120-149	Ettringite	Decomposition with water release
122, 200	Gypsum	Decomposition with water release
300-400	Brucite	Decomposition with water release
400-460	Portlandite	Decomposition with water release
551	Iowaite	Decomposition with water and CO2 release.
573	Quartz	α to β polymorphic transformation (crystal structure change)
620-690	Calcite	Typical decomposition for cryptocrystalline calcite formed due to in-situ carbonation of mortars.
680-800	Calcite	Typical decomposition for coarsely crystalline calcite in rock lime (as limestone) and marine shells.

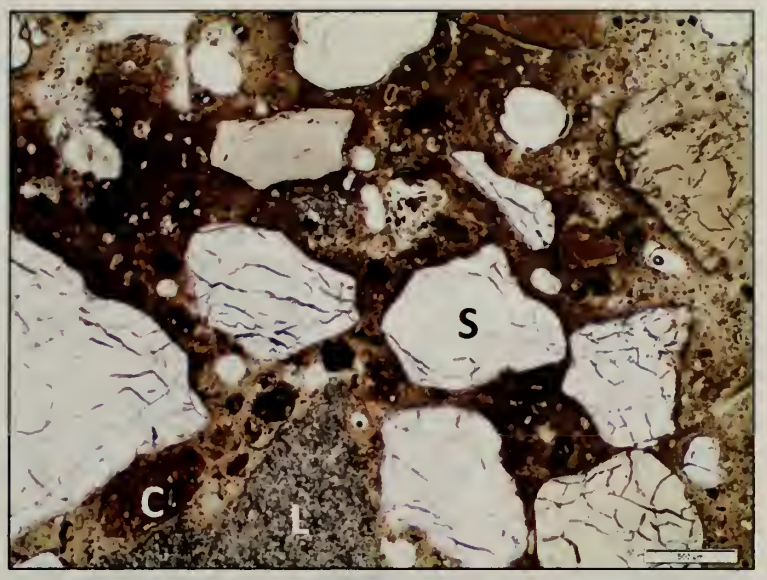

Figure 14: Microstructure of Mortar 3-1-14 with Cement Particles in Matrix PPL

Microstructural Features: Sand (S), cementitious matrix (M), Pores (P), Lime relic (R) and Cement relic (C); PPL=plane polarized transmitted light and XPL=transmitted light crossed nicols.

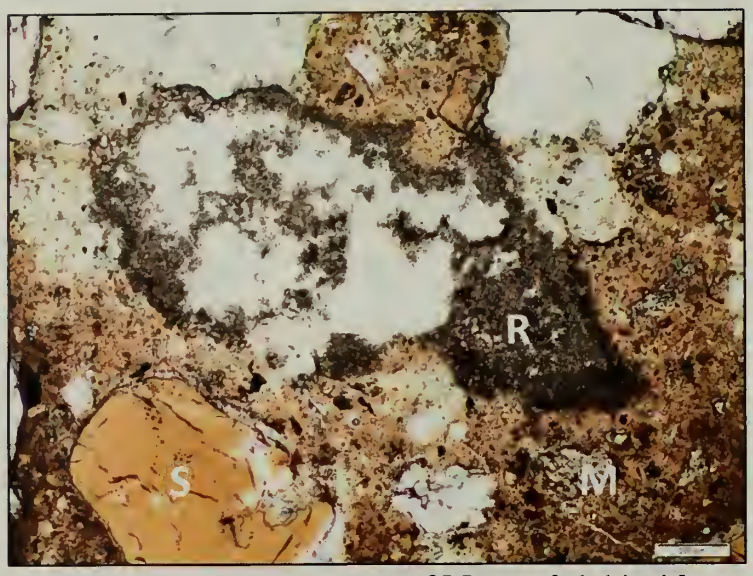

Figure 15: Microstructure of Mortar 3-1-14 with Lime Agglomerate PPL

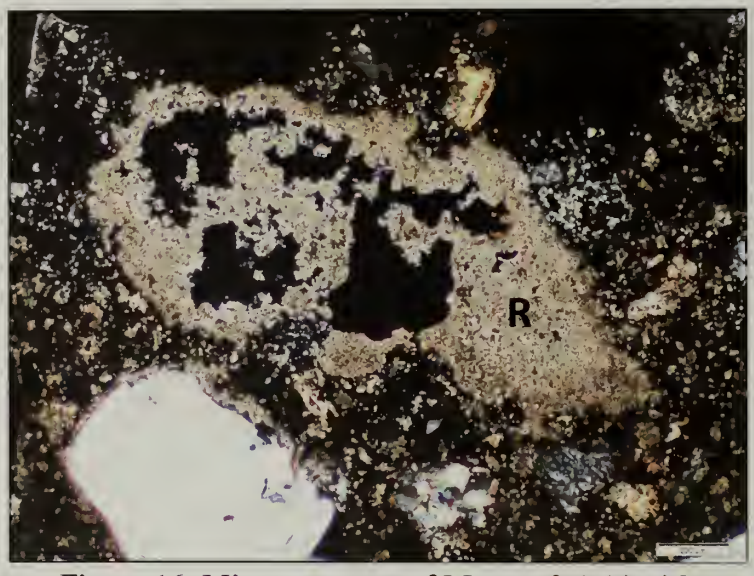

Figure 16: Microstructure of Mortar 3-1-14 with Lime Agglomerate XPL

Microstructural Features: Sand (S), cementitious matrix (M), Pores (P), Lime relic (R) and Cement relic (C); PPL=plane polarized transmitted light and XPL=transmitted light crossed nicols.

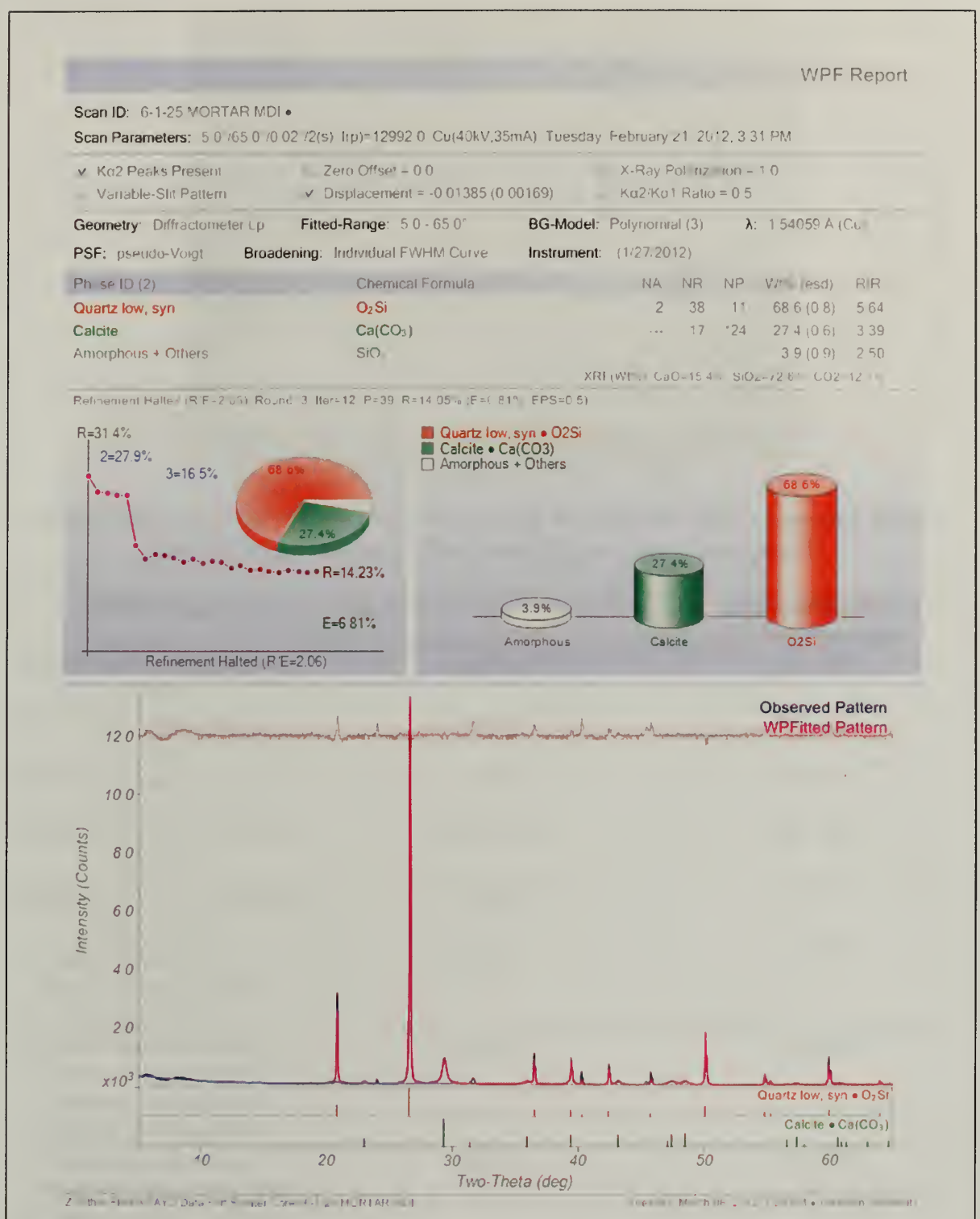

Figure 17: XRD of Mortar 6-1-25

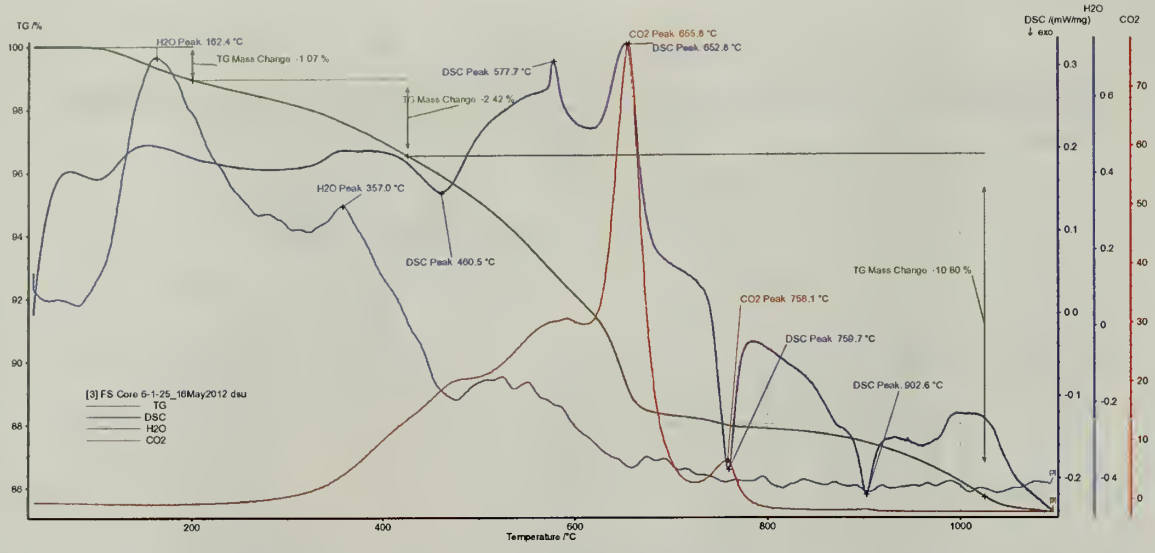

Figure 18: TGA/EGA of Mortar 6-1-25

Typical Thermal Events Observed in Thermal Analysis of Historic Bricks and Mortars (These events serve as a "fingerprint" for mineral identification)

Event Temperature (Approximate, °C)	Mineral Species Involved	Type of Event
120-149	Ettringite	Decomposition with water release
122, 200	Gypsum	Decomposition with water release
300-400	Brucite	Decomposition with water release
400-460	Portlandite	Decomposition with water release
551	Iowaite	Decomposition with water and CO2 release.
573	Quartz	α to β polymorphic transformation (crystal structure change)
620-690	Calcite	Typical decomposition for cryptocrystalline calcite formed due to in-situ carbonation of mortars.
680-800	Calcite	Typical decomposition for coarsely crystalline calcite in rock lime (as limestone) and marine shells.

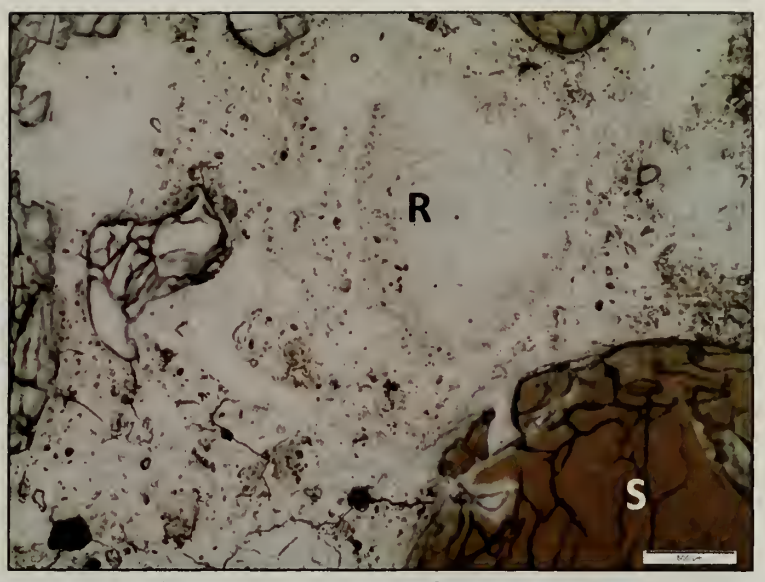

Figure 19: Microstructure of Mortar 6-1-25 with Calcareous Matric and Lime Agglomerate PPL

Microstructural Features: Sand (S), cementitious matrix (M), Pores (P), Lime relic (R) and Cement relic (C); PPL=plane polarized transmitted light and XPL=transmitted light crossed nicols.

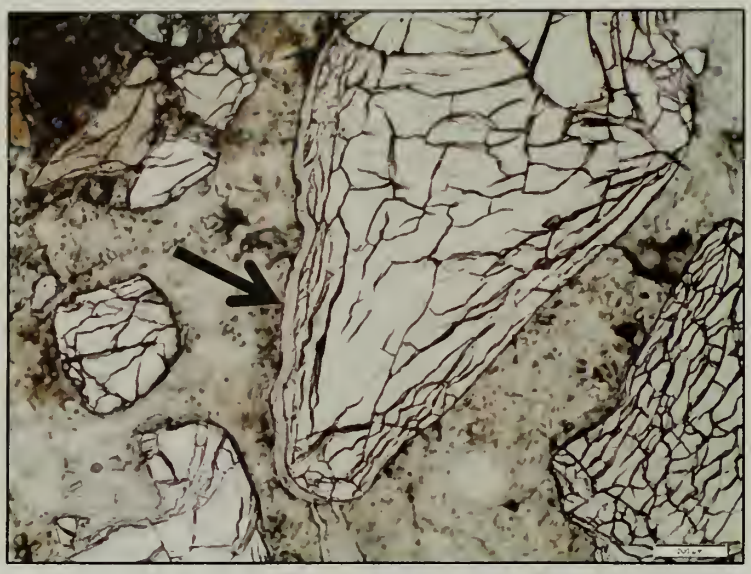

Figure 20: Microstructure of Mortar 6-1-25 with Peripheral Crack (arrow) around Quartz Due to ASR PPL

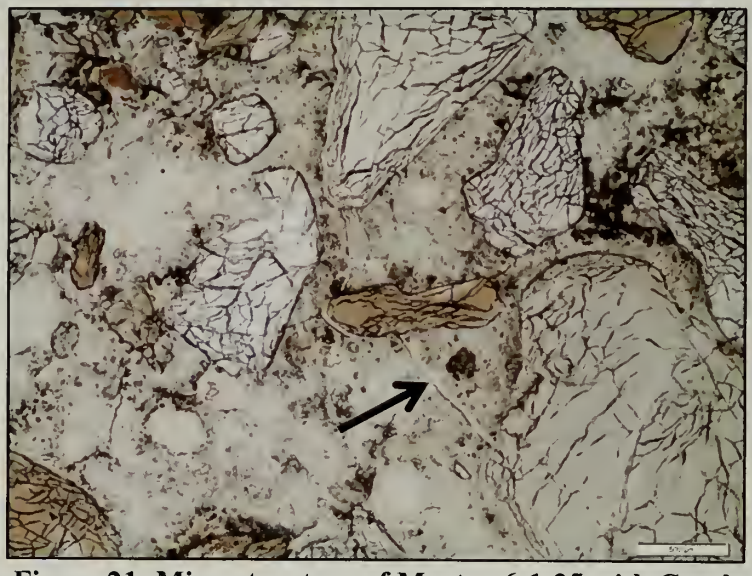

Figure 21: Microstructure of Mortar 6-1-25 with Crack Extension (arrow) Involving ASR PPL

Microstructural Features: Sand (S), cementitious matrix (M), Pores (P), Lime relic (R) and Cement relic (C); PPL=plane polarized transmitted light and XPL=transmitted light crossed nicols.

Figure 22: Microstructure of Mortar 6-1-25 Crack Extension through Quartz (arrow) PPL

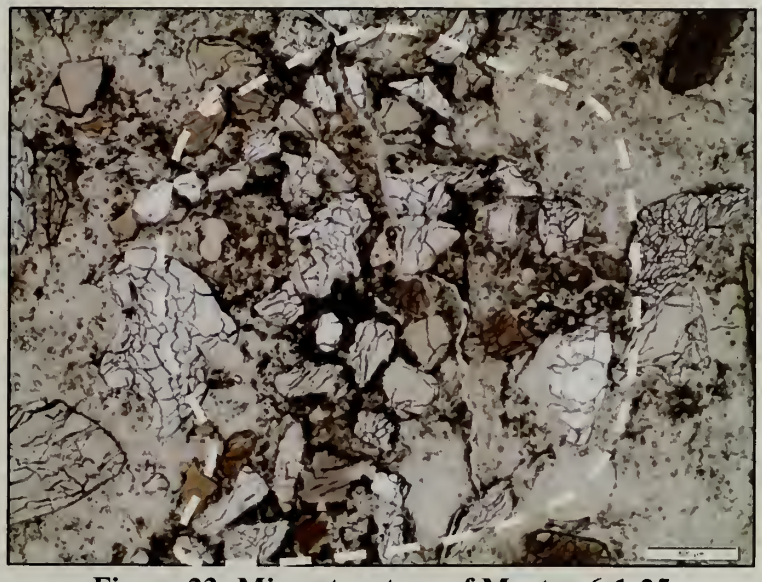

Figure 23: Microstructure of Mortar 6-1-25 Exhibiting Corrosion (within dashed line) PPL

Microstructural Features: Sand (S), cementitious matrix (M), Pores (P), Lime relic (R) and Cement relic (C); PPL=plane polarized transmitted light and XPL=transmitted light crossed nicols.

Figure 24: XRD of Tabby Concrete 4-2-22

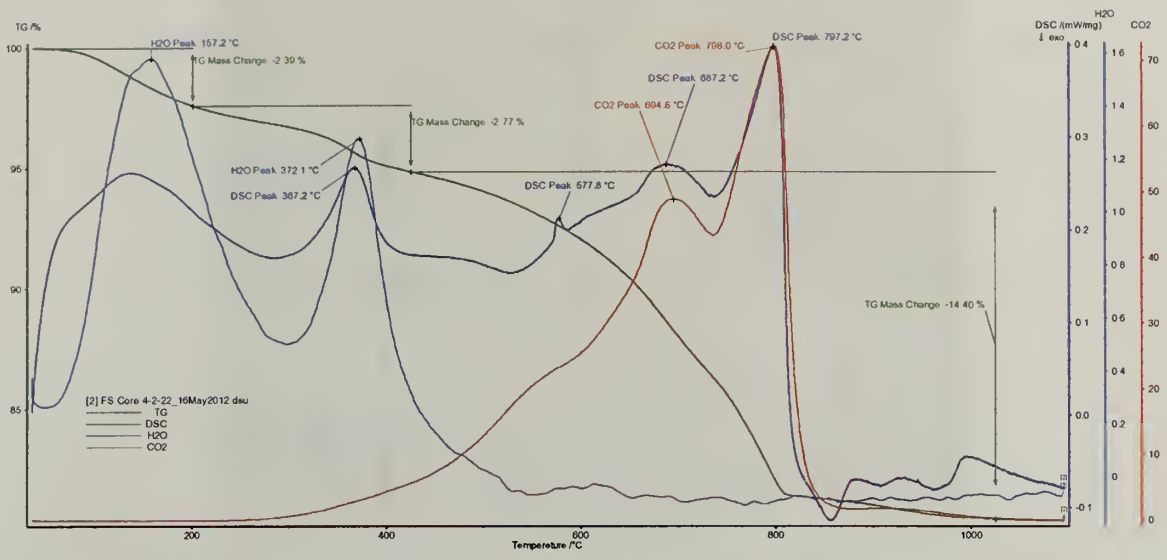

Figure 25: TGA/EGA of Tabby Concrete 4-2-22

Typical Thermal Events Observed in Thermal Analysis of Historic Bricks and Mortars (These events serve as a "fingerprint" for mineral identification)

Event Temperature (Approximate, °C)	Mineral Species Involved	Type of Event
120-149	Ettringite	Decomposition with water release
122, 200	Gypsum	Decomposition with water release
300-400	Brucite	Decomposition with water release
400-460	Portlandite	Decomposition with water release
551	Iowaite	Decomposition with water and CO2 release.
573	Quartz	α to β polymorphic transformation (crystal structure change)
620-690	Calcite	Typical decomposition for cryptocrystalline calcite formed due to in-situ carbonation of mortars.
680-800	Calcite	Typical decomposition for coarsely crystalline calcite in rock lime (as limestone) and marine shells.

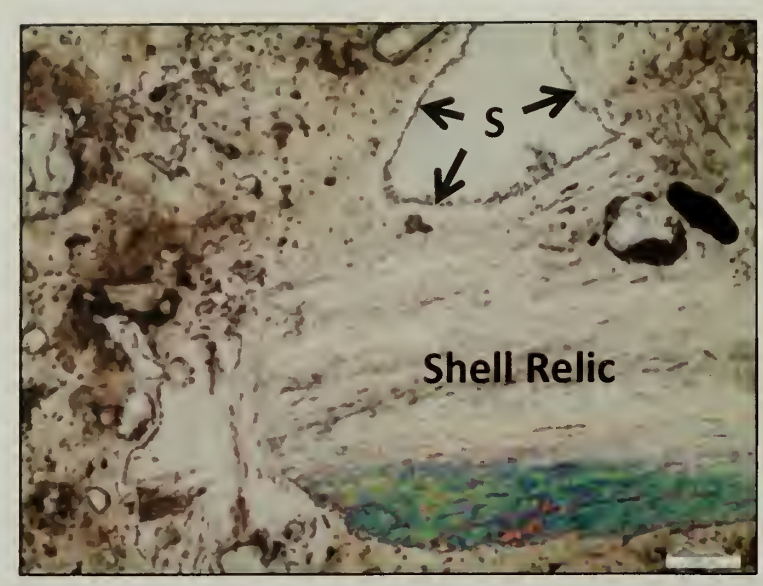

Figure 26: Microstructure of 6 Tabby Concrete 4-2-22 with Matrix and Shell with ASR (arrow) on Quartz PPL

Microstructural Features: Sand (S), cementitious matrix (M), Pores (P), Lime relic (R) and Cement relic (C); PPL=plane polarized transmitted light and XPL=transmitted light crossed nicols.

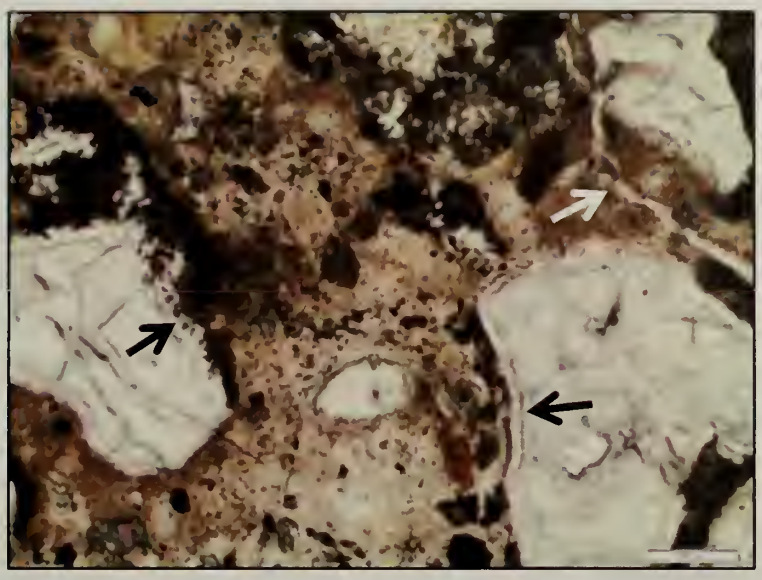

Figure 27: Microstructure of Tabby Concrete 4-2-22 with Detail of ASR (arrows) PPL

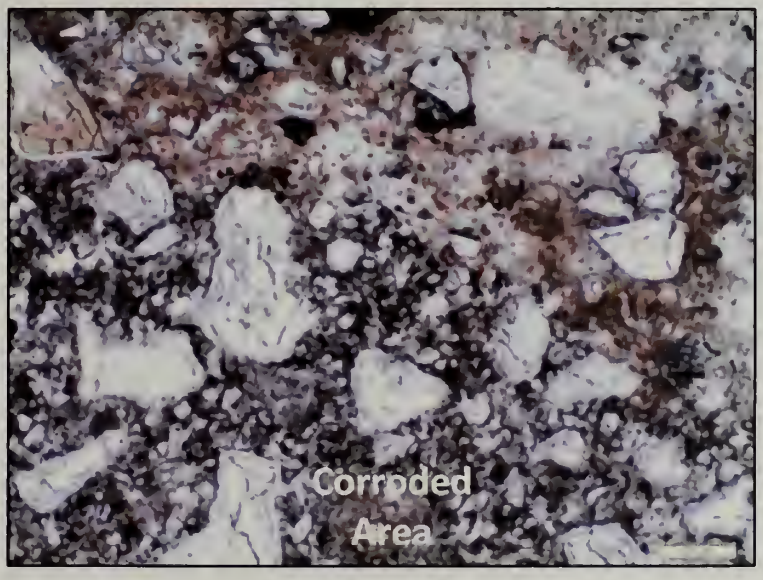

Figure 28: Microstructure of Tabby Concrete 4-2-22 with Stained and Corroded Area Lower Left PPL

Microstructural Features: Sand (S), cementitious matrix (M), Pores (P), Lime relic (R) and Cement relic (C); PPL=plane polarized transmitted light and XPL=transmitted light crossed nicols.

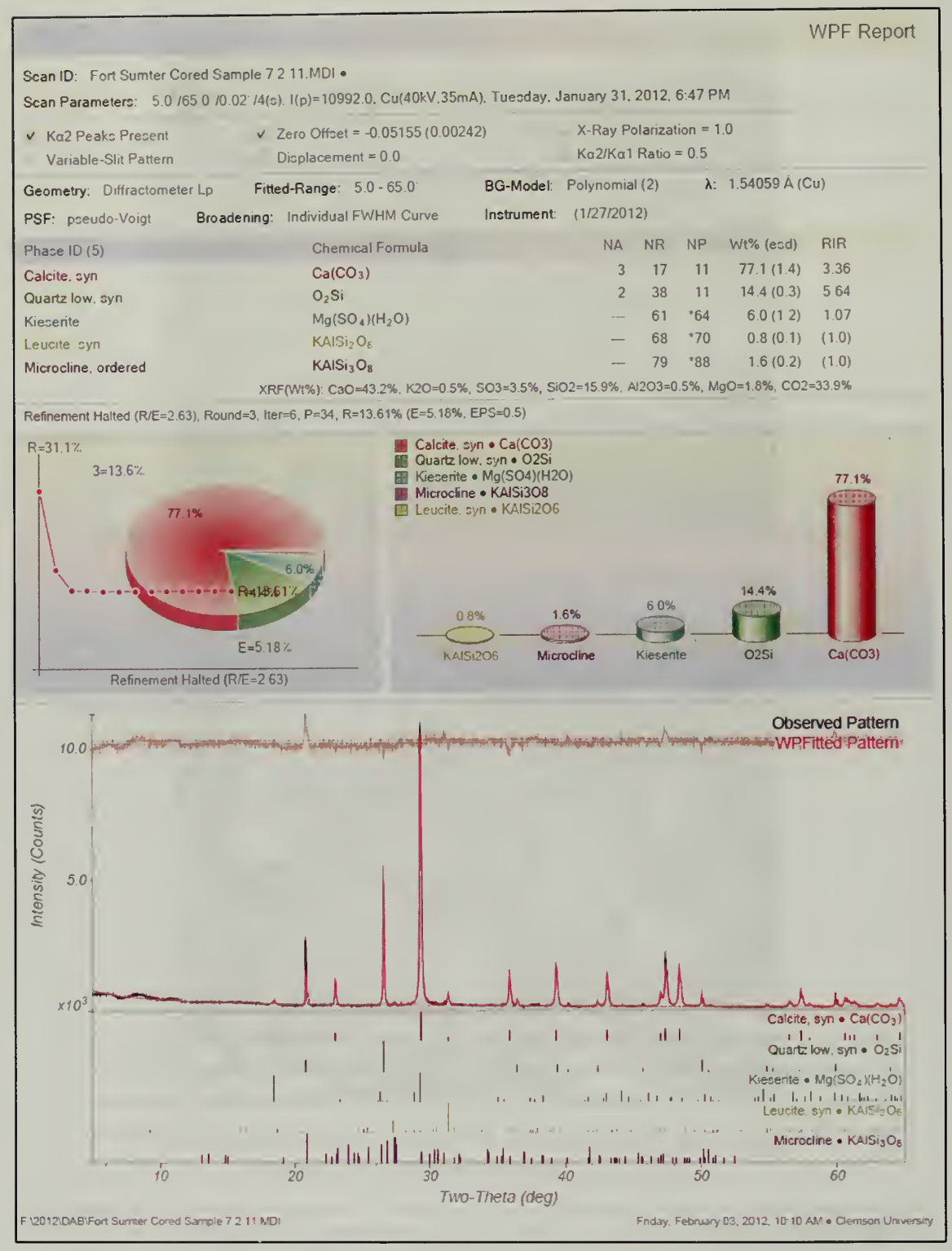

Figure 29: XRD of Tabby Concrete 7-2-1

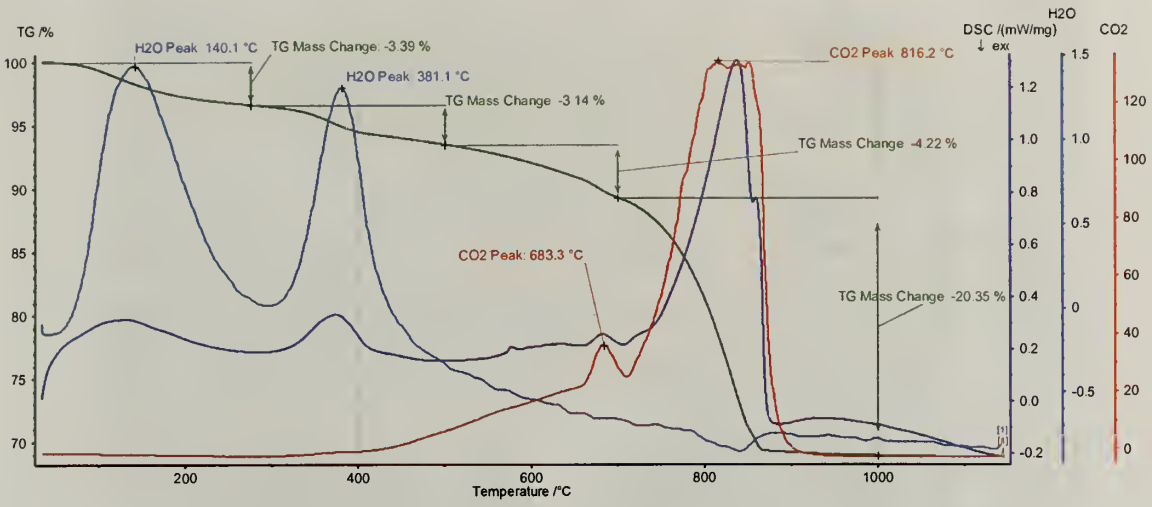

Figure 30: TGA/EGA of Tabby Concrete 7-2-1

Typical Thermal Events Observed in Thermal Analysis of Historic Bricks and Mortars (These events serve as a "fingerprint" for mineral identification)

Event Temperature (Approximate, °C)	Mineral Species Involved	Type of Event
120-149	Ettringite	Decomposition with water release
122, 200	Gypsum	Decomposition with water release
300-400	Brucite	Decomposition with water release
400-460	Portlandite	Decomposition with water release
551	Iowaite	Decomposition with water and CO2 release.
573	Quartz	α to β polymorphic transformation (crystal structure change)
620-690	Calcite	Typical decomposition for cryptocrystalline calcite formed due to in-situ carbonation of mortars.
680-800	Calcite	Typical decomposition for coarsely crystalline calcite in rock lime (as limestone) and marine shells.

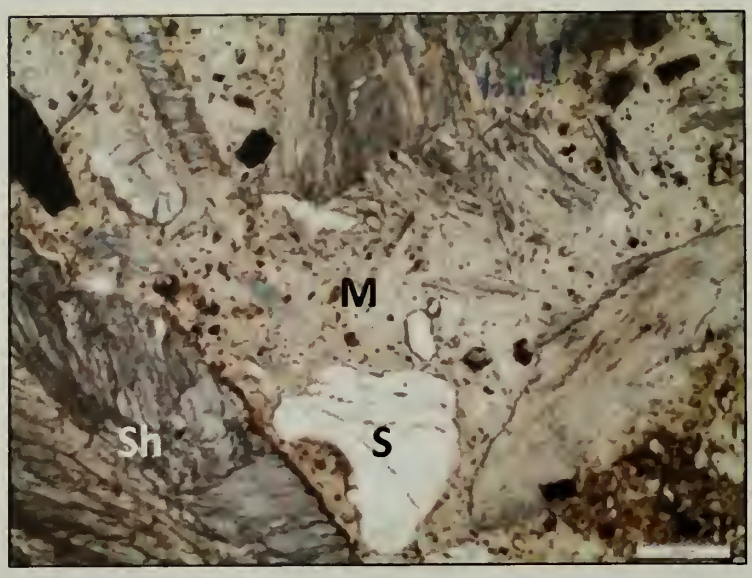

Figure 31: Microstructure of Tabby Concrete 7-2-1 with Matrix Stained Area (lower right) PPL

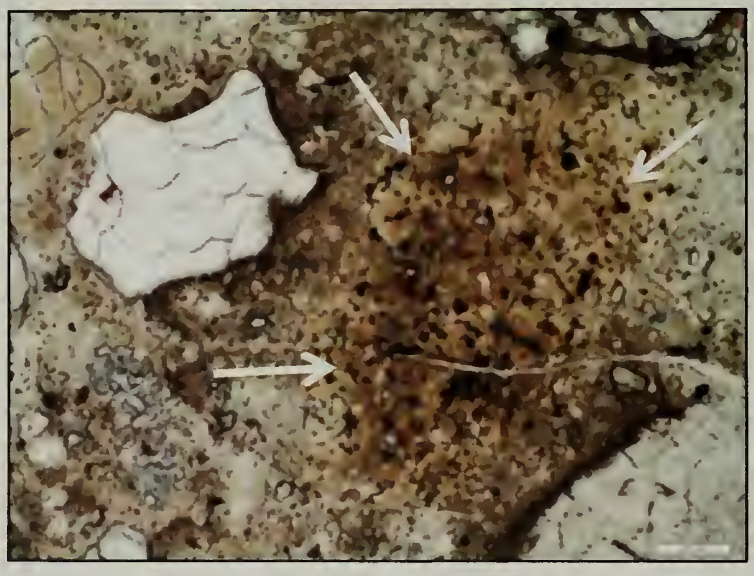

Figure 32: Microstructure of Tabby Concrete 7-2-1 with Brick Dust Stained Area (lower right, arrows) PPL

Microstructural Features: Sand (S), cementitious matrix (M), Pores (P), Lime relic (R) and Cement relic (C); PPL=plane polarized transmitted light and XPL=transmitted light crossed nicols.

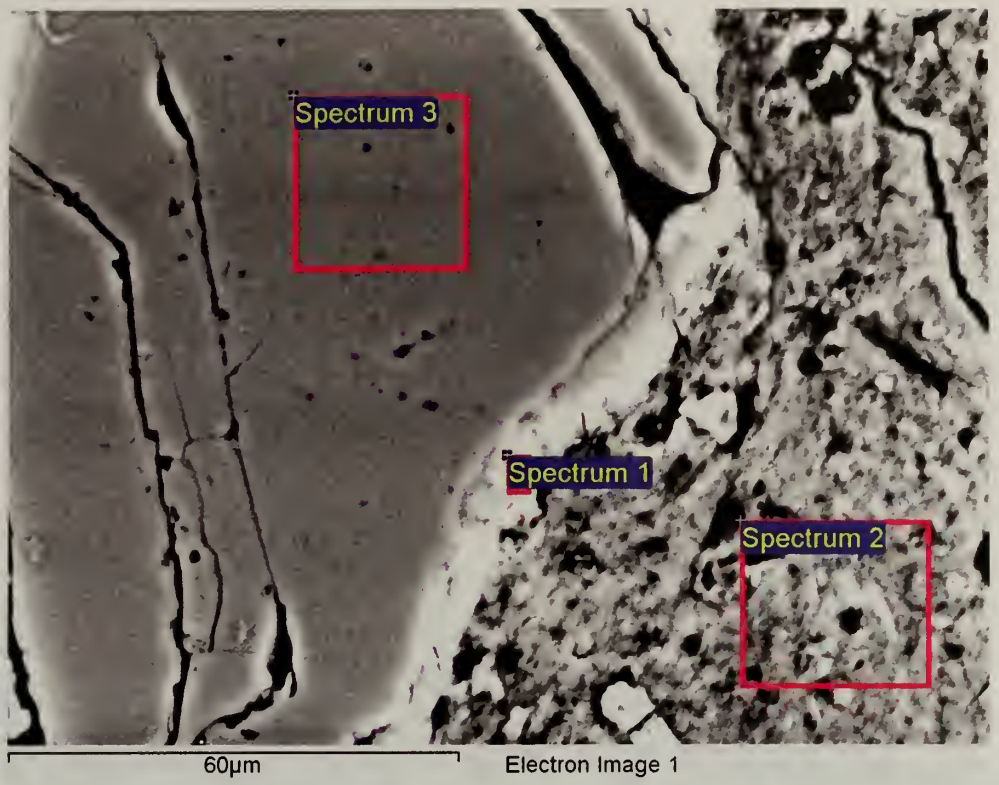

Figure 33: SEM Microstructure of Tabby Concrete 7-2-1 with ASR at Quartz Grain Periphery

Table 3: EDAX Chemical Analysis of Areas in Figure 33 (Oxidized Basis)

Composition	Spectrum 1	Spectrum 2	Spectrum 3
Identity of area within spectrum	Edge of sand particle (quartz)	Cementitious matrix	Sand particle (quartz)
CaO	43.70	36.04	2.35
MgO	1.53	18.25	1.15
Al_2O_3	1.71	4.18	0
Fe_2O_3	0	2.09	0
SiO_2	53.04	36.53	96.50
S	0	0.84	0
Cl	0	.1.01	0
Sum	99.98	98.04	100

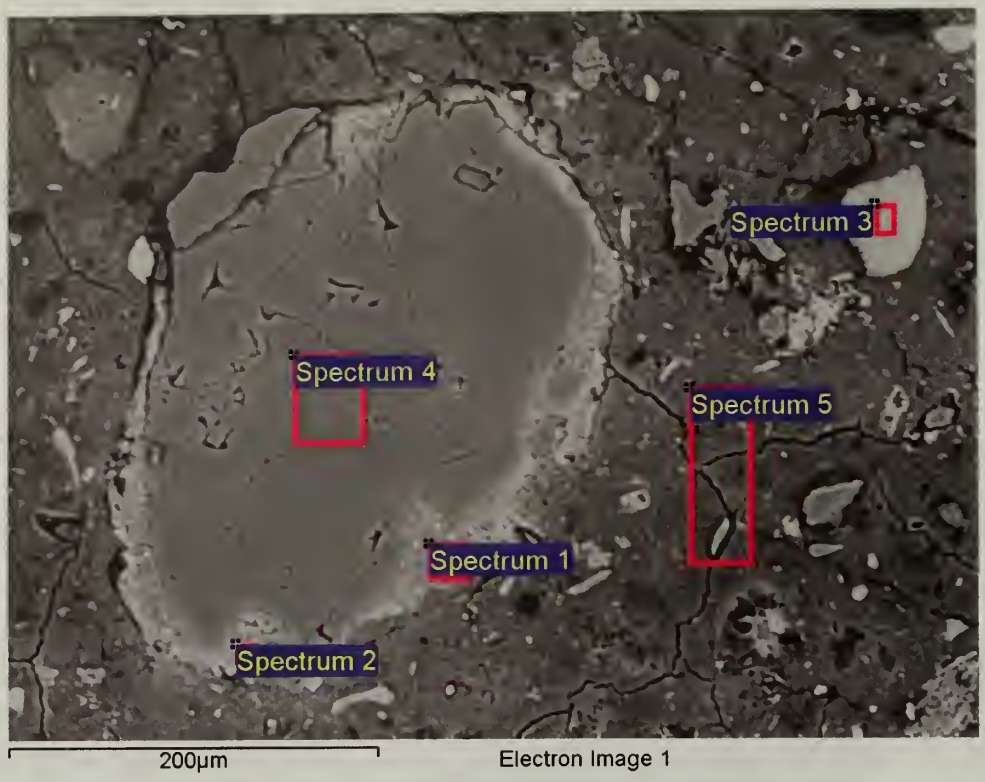

Figure 34: SEM Microstructure of 7-2-1 with ASR at Quartz Grain Periphery And Crack Extension in the Tabby Concrete Matrix

Table 4: EDAX Chemical Analysis of Areas in Figure 34 (Oxidized Basis)

	Spectrum 1	**Spectrum 2**	**Spectrum 3**	**Spectrum 4**	**Spectrum 5**
Identity of area within spectrum	Edge of sand particle (quartz)	Edge of sand particle (quartz)	Shell fragment	Sand (quartz)	Cementitious matrix
CaO	16.80	38.10	93.32	1.71	33.49
MgO	1.24	1.88	1.58	0.53	20.85
Al_2O_3	20.40	12.07	0.88	0	4.06
Fe_2O_3	3.23	2.87	0	0	2.41
SiO_2	57.64	45.08	4.22	97.76	36.25
Na_2O	0.66	0	0	0	0
S	0	0	0	0	0.52
Cl	0	0	0	0	2.39
Sum	99.97	100	100	100	99.97

Figure 35: Brick Specimen 2-1-1

Figure 36: Brick Specimen 2-1-2

Figure 37: Brick Specimen 3-1-14 (upper)

Figure 38: Brick Specimens 3-1-17
(Left to Right – Grey Brick, Grey Brick with Mortar, Red Brick)

Figure 39: Brick Specimens 6-1-25
(Center Specimen is Tabby Concrete)

Figure 40: Brick Specimen 7-1-9

Table 5: Brick Analytical Data Summary

	2-1-1	2-1-2	3-1-14	3-1-17 Dark	3-1-17 Red	6-1-25	7-1-9
Brick Type	Grey	Grey	Grey	Grey	Grey	Brown	Grey
Bulk XRF							
Al_2O_3	5.70	3.29	8.15	8.15	5.50	5.01	9.08
SiO_2	92.54	92.32	85.70	85.70	87.44	87.29	83.78
Na_2O	<0.5	<0.5	<0.5	<0.5	<0.5	<0.5	<0.5
K_2O	0.40	0.60	0.88	0.88	1.00	1.30	0.71
MgO	0.40	<0.2	0.45	0.45	0.30	0.20	0.49
CaO	<0.01	<0.01	0.10	0.10	0.20	0.20	0.57
TiO_2	0.20	0.70	1.03	1.03	1.30	1.50	0.90
MnO	<0.005	0.02	0.03	0.03	0.03	0.04	0.03
Fe_2O_3	0.60	2.50	3.40	3.40	3.80	4.10	4.20
P_2O_5	0.10	0.30	0.08	0.08	0.20	0.20	0.08
S	<0.05	<0.05	<0.05	<0.05	<0.05	<0.05	<0.05
LOI	0.26	1.25	0.16	0.47	0.37	0.54	0.69
XRD, %							
Cristobalite	2.5	2.9	5.4	7.8	8.2	8.6	12.2
Tridymite	36.8	36.1	55.3	38.4	40.6	48.9	38.0
Quartz	32.0	50.7	21.6	45.2	32.8	27.7	31.7
Total SiO_2	71.3	89.7	82.3	91.4	81.6	85.2	81.9
Mullite	5.8	7.4	7.0	-	5.9	5.4	12.2
Amorphous + Other	22.8	2.9	9.0	5.1	12.5	9.4	5.9
Hematite	-	-	1.7	3.6	-	-	
Thermal Expansion, CTE X exp6 /K	12.6	11.7	11.8	10.8	9.8	12.6	na
Soluble Salts, ppm of dry specimen							
Na	158	142	123	158	148	915	86
K	100	76	31	520	140	171	128
Mg	84	45	36	25	47		34
Ca	134	75	113	173	271	298	550
Cl	152	115	53	116	122	1287	14
NO_2							
SO_4	12	5.5	3	18	13	91	65
Bulk density, g/cm^3	1.54	1.55	1.64	1.66	1.60	1.61	1.67
Apparent Porosity	38.9	41.0	34.0	33.4	35.2	32.2	31.6
Fraction of pores <1 micron	0.9	1.8	3.2	4.8	2.2	2.4	3.4

Note: There was insufficient specimen quantity for 4-1-20 analytical.

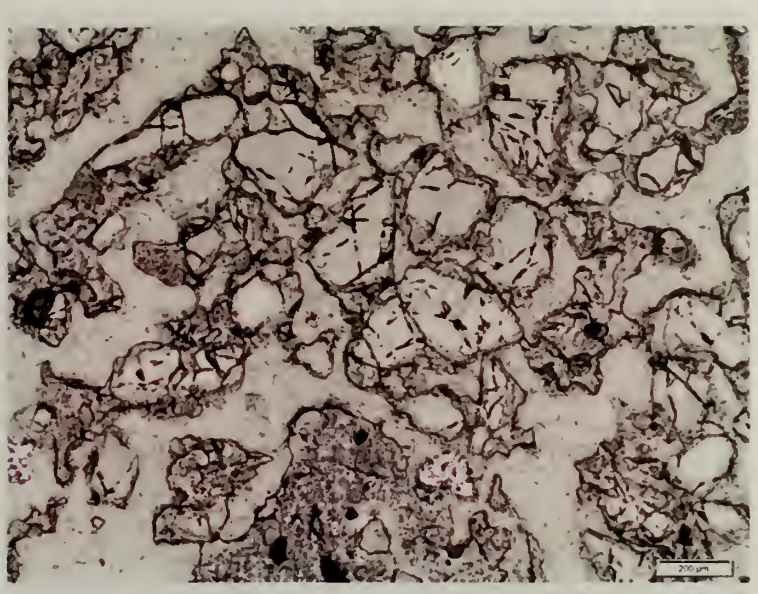

Figure 41: Microstructure of 2-1-1 Brick RPL (Same area as Figure 42)

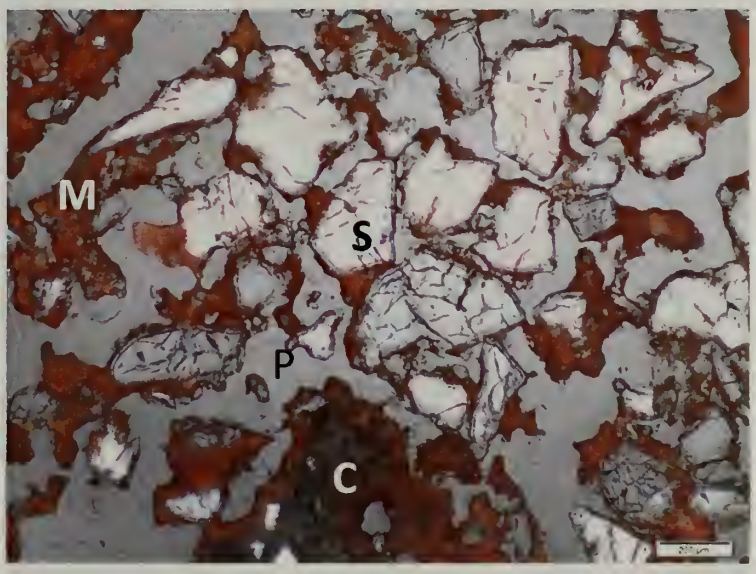

Figure 42: Microstructure of Brick 2-1-1 RXPL

Microstructural Features: Sand (S), Vitrified matrix (M),
Pores (P), and Chert nodule (C); RPL = reflected polarized light and RPXL = reflected light crossed nicols.

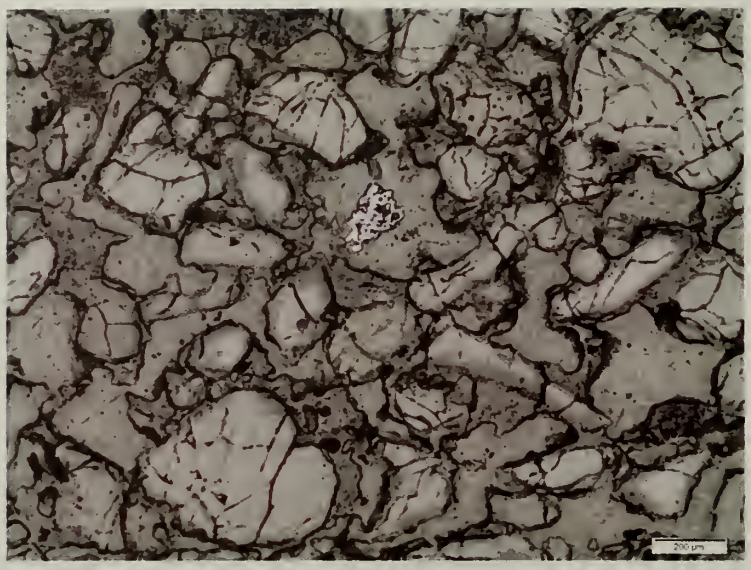

Figure 43: Microstructure of Brick 2-1-2 RPL (Same area as Figure 44)

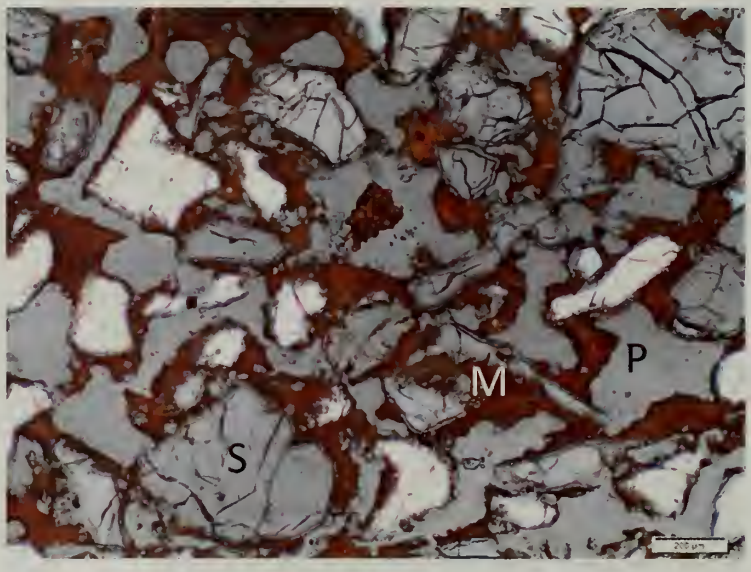

Figure 44: Microstructure of Brick 2-1-2 RXPL

Microstructural Features: Sand (S), Vitrified matrix (M),
Pores (P), and Chert nodule (C); RPL = reflected polarized light and RPXL = reflected light crossed nicols.

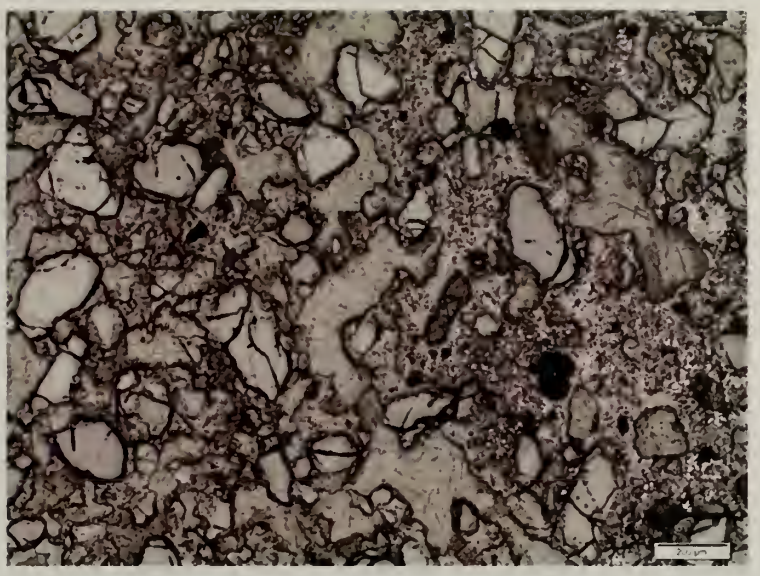

Figure 45: Microstructure of Brick 3-1-17 RPL (Same area as Figure 46) (Chert Nodule to Right of Field)

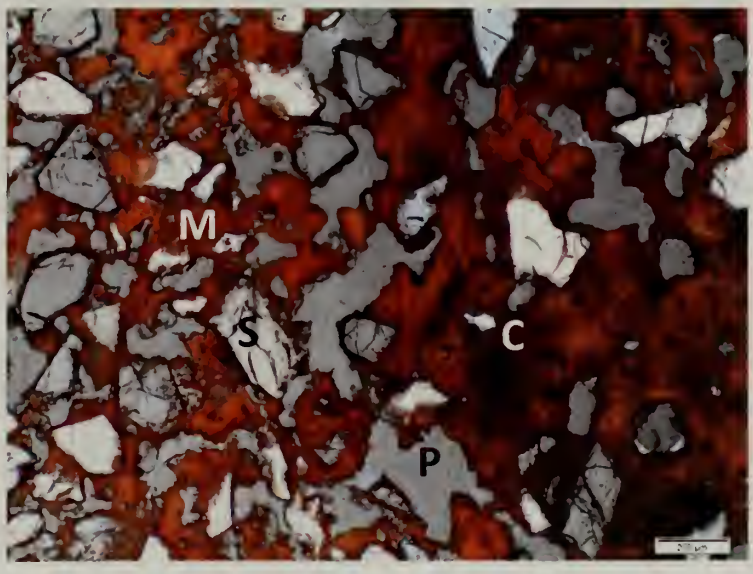

Figure 46: Microstructure of Brick 3-1-17 RXPL (Chert Nodule to Right of Field)

Microstructural Features: Sand (S), Vitrified matrix (M), Pores (P), and Chert nodule (C); RPL = reflected polarized light and RPXL = reflected light crossed nicols.

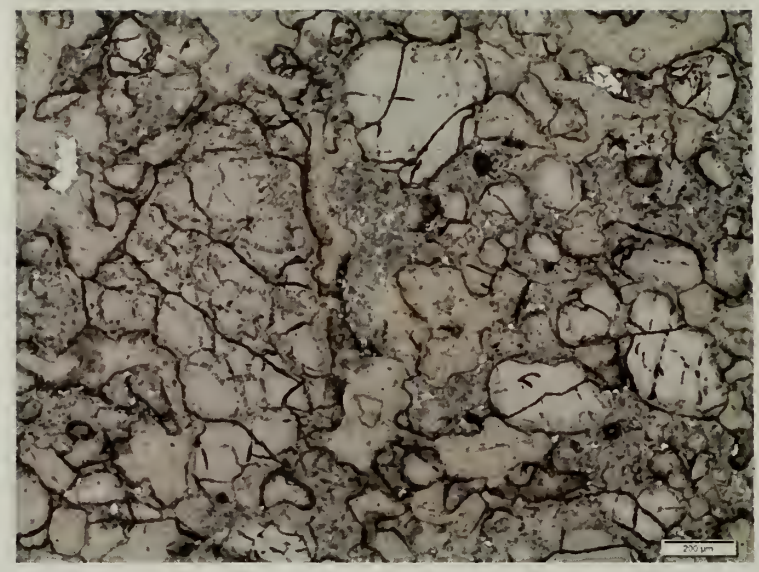

Figure 47: Microstructure of Brick 3-1-19 RPL (Same area as Figure 48)

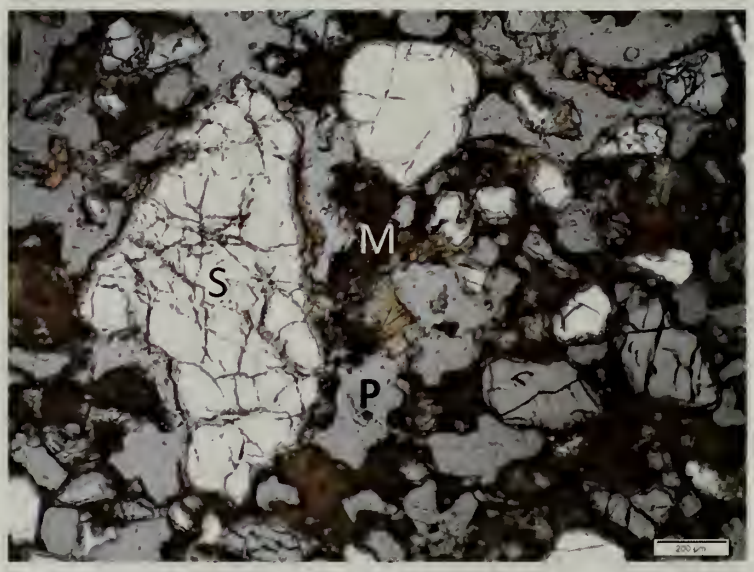

Figure 48: Microstructure of Brick 3-1-19 RXPL

Microstructural Features: Sand (S), Vitrified matrix (M),
Pores (P), and Chert nodule (C); RPL = reflected polarized light and RPXL = reflected light crossed nicols.

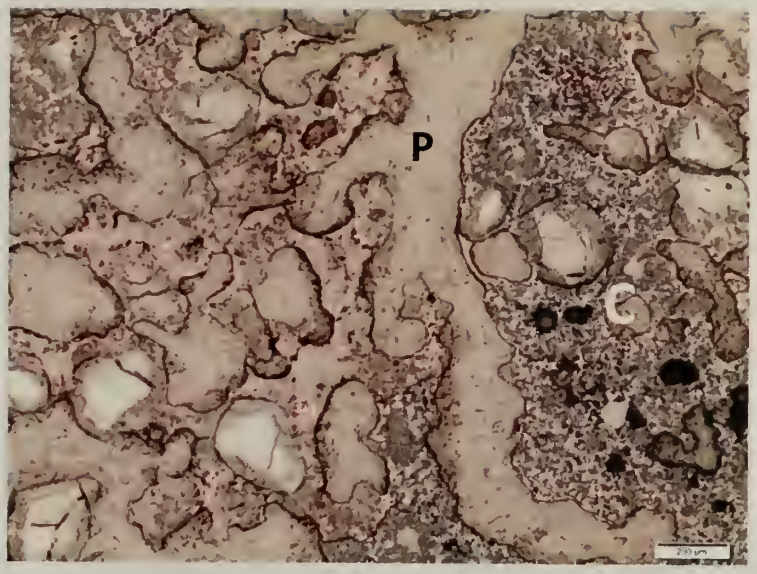

Figure 49: Microstructure of Brick 4-1-20 RPL

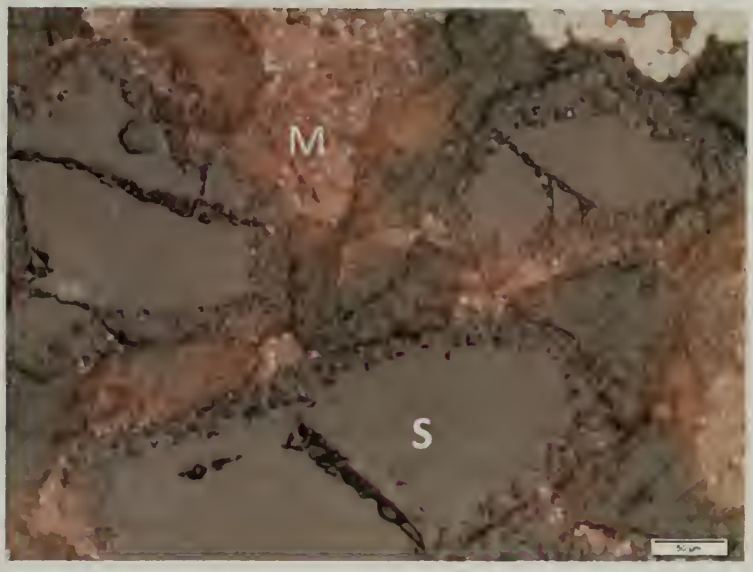

Figure 50: Microstructure of Brick 4-1-20 RXPL

Microstructural Features: Sand (S), Vitrified matrix (M),
Pores (P), and Chert nodule (C); RPL = reflected polarized light and RPXL = reflected light crossed nicols. No analytical measurements were made on Core 4-1-20 bricks.

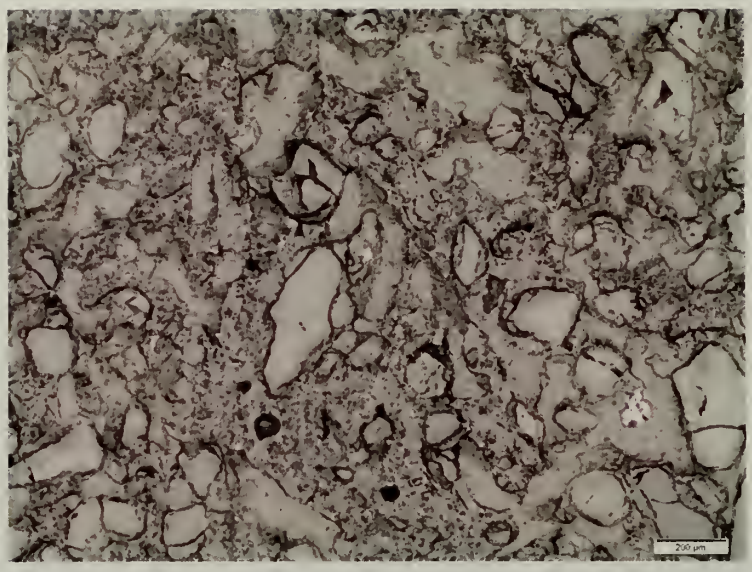

Figure 51: Microstructure of Brick 6-1-25 RPL (Same field as Figure 52)

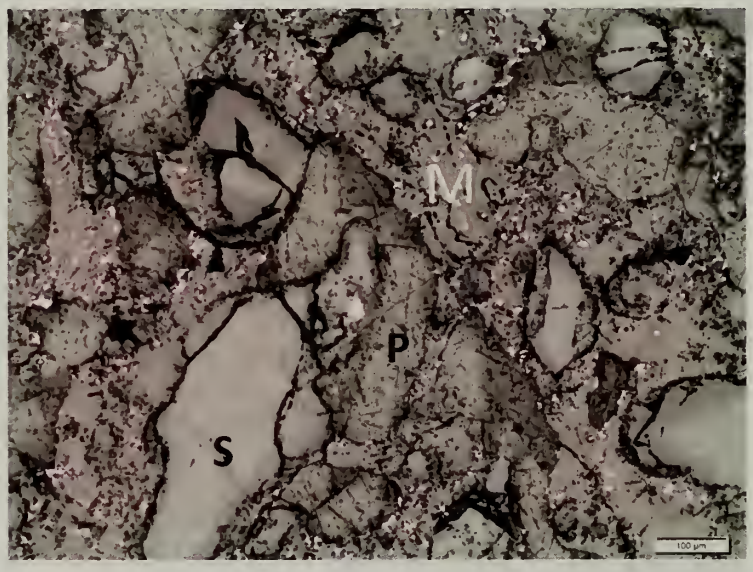

Figure 52: Microstructure of Brick 6-1-25 RXPL

Microstructural Features: Sand (S), Vitrified matrix (M),
Pores (P), and Chert nodule (C); RPL = reflected polarized light and RPXL = reflected light crossed nicols.

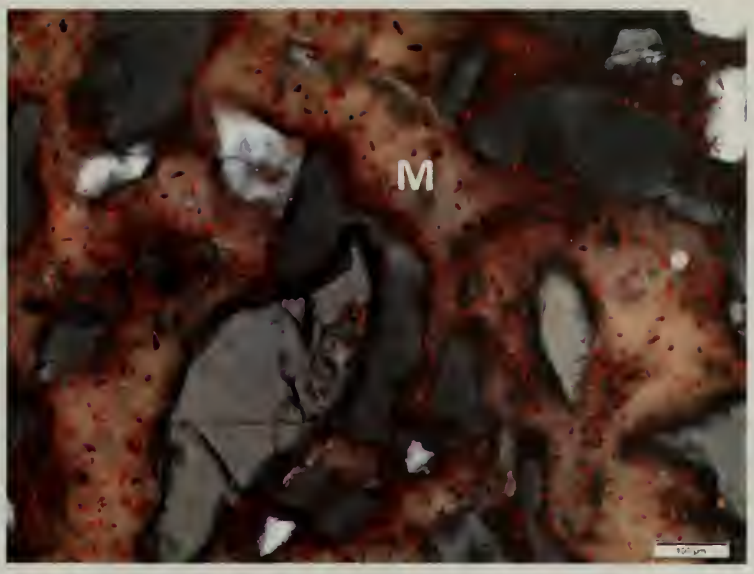

Figure 53: Detail of Brick Matrix of 6-1-25 RPL

Microstructural Features: Sand (S), Vitrified matrix (M),
Pores (P), and Chert nodule (C); RPL = reflected polarized light and RPXL = reflected light crossed nicols.

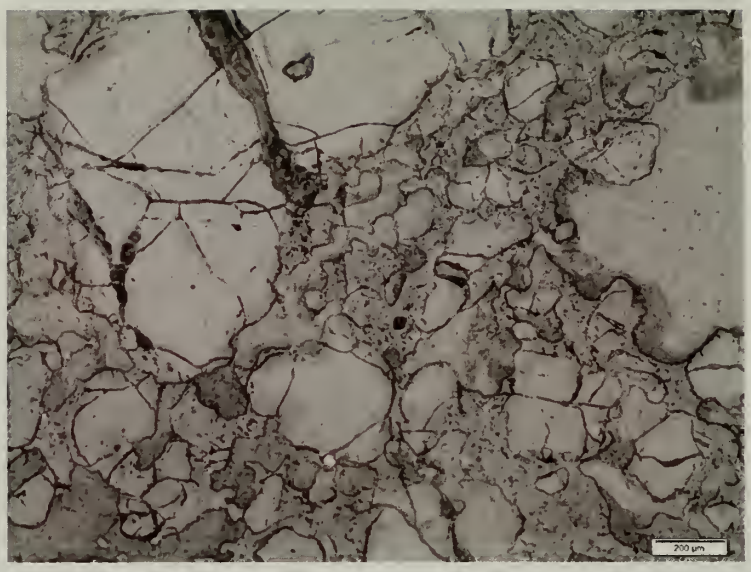

Figure 54: Microstructure of Brick 7-1-9 RPL (Same field as Figure 55)

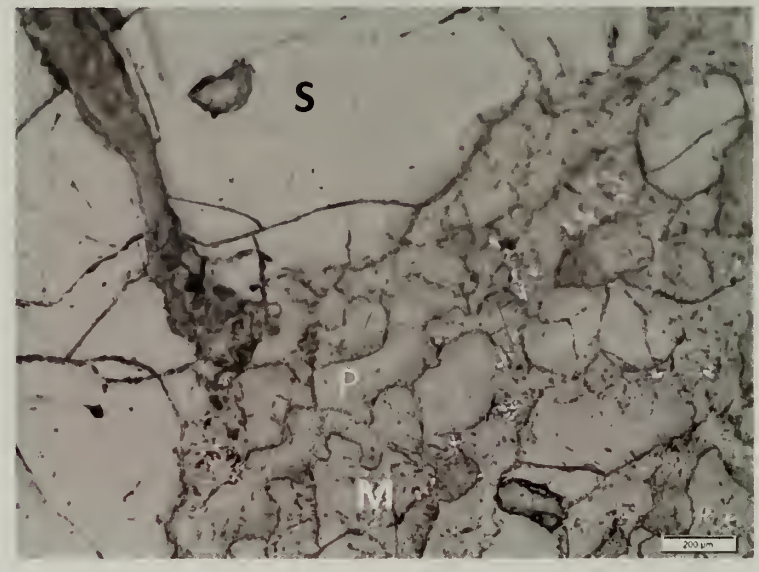

Figure 55: Detail of Brick 7-1-9 RPL
(Scale Bar should indicate 100μ)

Microstructural Features: Sand (S), Vitrified matrix (M),
Pores (P), and Chert nodule (C); RPL = reflected polarized light and RPXL = reflected light crossed nicols.

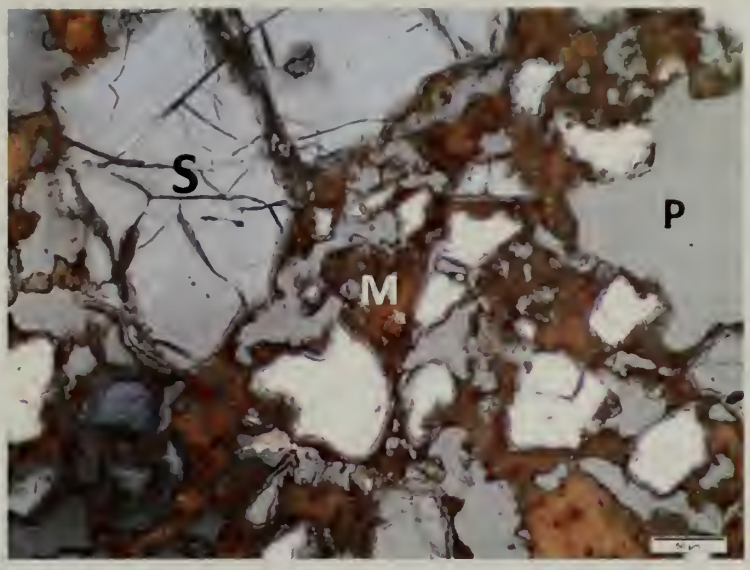

Figure 56: Detail of Brick Matrix of 7-1-9 RXPL

Microstructural Features: Sand (S), Vitrified matrix (M),
Pores (P), and Chert nodule (C); RPL = reflected polarized light and RPXL = reflected light crossed nicols.